CO_2 Sequestration in Red Mud-GGBS Geopolymers: Impacts on Strength and Microstructure

Rani Ravichandran[1] and Shanmugasundaram Muthusamy[2*]

[1]Research Associate, School of Civil Engineering, Vellore Institute of Technology, Chennai – 600127.

[2*]Associate Professor, School of Civil Engineering, Vellore Institute of Technology, Chennai – 600127.

*Corresponding author's e-mail - shanmuga.sundaram@vit.ac.in

Graphical Abstract:

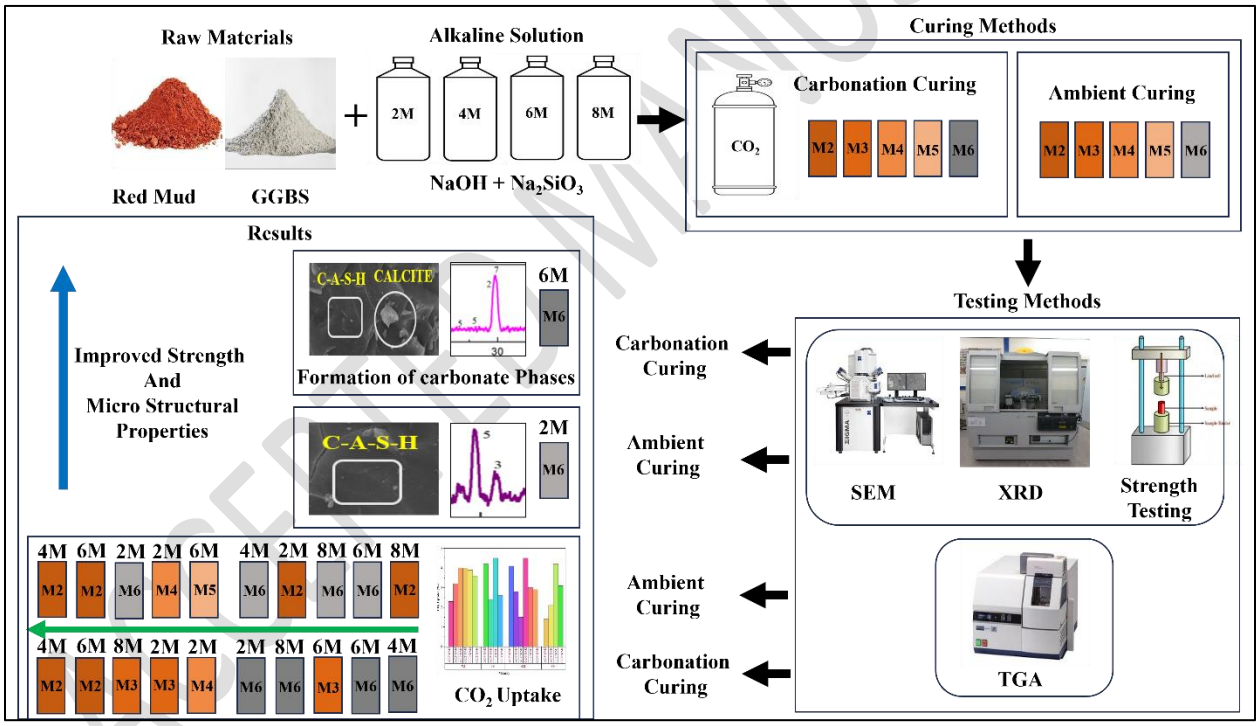

ABSTRACT

Currently the focus on the mitigation of CO_2 emissions is receiving great appreciation worldwide through the use of different technologies. Mineral carbonation technology was employed for CO_2 fixation using industrial byproducts such as Red Mud (RM) and Ground Granulated Blast Furnace Slag (GGBS) as precursor materials. The sustainable utilization of these industrial byproducts in geopolymers used two different curing regimes such as carbonation curing and ambient curing to evaluate the effect of CO_2 exposure on binder performance. The strength and micro structural properties were observed by testing compressive strength, X-ray diffraction (XRD) and Scanning Electron Microscopy (SEM) analyses. The carbon sequestration potential of the binder material was determined using CO_2 uptake values derived from thermogravimetric analysis (TGA). These analyses confirmed carbon fixation within the binder material during curing. This study ensures the solidification of geopolymers without any CO_2 emissions and uptake of carbon to improve mechanical strength. Ambient-cured samples were used to determine the reliable strength gain and better micro-structural development of carbonated samples. The results indicated the advantages of integrating mineral carbonation for CO_2 sequestration with carbonation curing, leading to an overall reduction in the carbon footprint and enhanced mechanical properties of the RM-GGBS based geopolymer paste relative to traditional ambient curing. Regardless of the molarities used in this study (2M, 4M, 6M and 8M) and curing conditions, GGBS-based samples performed well. In particular, the carbonation cured GGBS sample proved better mechanical strength, structural integrity and mitigation of carbonation induced degradation. The better CO_2 uptake observed in RM-rich mixes is attributed to their enhanced alkalinity, whereas GGBS-rich systems exhibit comparatively moderate carbonation capacity.

Keywords: Red mud (RM), Ground granulated Blast Furnace Slag (GGBS), Geopolymer, Carbonation curing, Ambient curing, Compressive strength, Micro structural analysis, CO_2 uptake

1. Introduction

Traditional concrete is the most popular artificial building material in the world; however, its sustainability is still a concern because cement production emits carbon dioxide, which contributes to the greenhouse effect (Tripathy & Acharya, 2023; Xia et al., 2025). Scientists are concerned about the environmental effects of using Portland cement as a binder in conventional concrete due to 5 % to 8 % carbon emissions worldwide and high energy consumption (Zhang et al., 2025b) occurs during the calcination process and manufacture (Munir et al., 2023). Every year, 100 million of metric tons of cement production, accounts for 15 - 20 % development of cement kiln dust and carbon dioxide, which creates threat to the environment and contaminates air, surface water, and ground water. These actions contradict environmental principles and pose sustainability issues (Al-Bakri, Ahmed & Hefni, 2022).

The energy required to produce Portland cement is high because the clinker must be fired at 1450º C. In the wet technique every ton of clinker production involves 5.8 tons of resources, which include air (3 tons), raw materials (1.6 tons), water (1 ton) and fuel (0.2 tons). The dry technique lowers the clinkers total to 4 tons by using air (2.3 tons), raw materials (1.6 tons) and fuel (0.1 tons) (Kuandykova et al., 2024). The intensity of water required for manufacturing cement ranges from 0.185 to 0.808 m^3/ton, according to research on direct water usage in the concrete sector (Ding et al., 2021)

Land fill problems and environmental issues can be prevented by using alternative cementitious materials such as slag, fly ash, red mud, metakaolin and rice husk ash in concrete, because of their chemical composition, which is similar to that of cement (Hongwei et al., 2025). Ground Granulated Blast Furnace Slag (GGBS) is a useful supplementary cementitious material since its pozzolanic and self-hydrating qualities and it's made up of 30 - 40 % calcium oxide. When such materials are added to concrete, the dependence on conventional components decreased without sacrificing strength, offering a sustainable substitute (Ahmad et al., 2022). Aluminium manufacturing produces red mud as a waste material when bauxite is subjected to alkaline treatment, resulting in reddish-brown color ascribed to iron oxide. 0.6 to 2.4 tons of red mud are created for every 1,000 kg of alumina. Globally, more than 600 million tons of red mud have accumulated (Ram Kumar & Ramakrishna, 2023).

Red mud can be used in place of cement in geopolymer concrete (GPC) because of its high alumina content, which also helps reduce red mud waste worldwide (John et al., 2016). The rise in atmospheric CO_2 caused by human activity is one of the primary causes of global warming, and it may be possible to keep this temperature increase between 2030 (Wang, Wu & Ma, 2024) and 2052 to 1.5º Celsius. To overcome this tendency, efforts have been made to create technologies for carbon collection, utilization and sequestration, as well as emission reduction strategies (Kopitha et al., 2025).

Carbon Capture, Utilization and Storage (CCUS) is a crucial method, that aims to mitigate greenhouse gas emissions and strives for climate change. Developing tailored solutions with lower carbon footprints has been the focus of recent research to reduce carbon emissions. This process creates carbonate ions when CO_2 dissolves in water, which subsequently reacts with the calcium and magnesium ions in the concrete. This makes it a more sustainable building material by increasing its potential to store carbon in concrete matrices, CO_2 fixation and storage are the subject of much current research (Wang & Fan, 2025).

Mineral carbonation is the most reliable method in CCUS technology for CO_2 sequestration, owing to its high alkalinity and abundance as a byproduct of the iron and steel industries, which eliminates CO_2 from the atmosphere and stabilizes and enhances the feedstock properties by addressing environmental and health issues associated with these materials (Wang, Kim & Qin, 2024). CO_2 capture and storage (CCS), is another main strategy by which effective CO_2 sequestration and waste conversion into mineral carbonates are possible with mineral

carbonation technology by transforming metal oxides (MeO) into stable carbonate crystals ($MeCO_3$) to collect and store CO_2 (Chandralega, Shanmugasundaram & Stone, 2025).

Carbonation Curing (CC) is a new technique for introducing CO_2 into cement-based materials. The metal carbonates formed by chemical reactions during the early hydration of CO_2 curing resulted in strength improvement and microstructural development in the hardened combination (Zhang et al., 2025a). Carbonation of materials containing calcium and magnesium can lower the CO_2 footprint and in sometimes CO_2 negative construction materials can be obtained (Winnefeld et al., 2022).

The introduction of geopolymer concrete, which demonstrated ceramic qualities similar to cement and was therefore approved as a cement substitute binder, is a better way to achieve sustainable concrete and reduce carbon emissions (Das et al., 2022). With the presence of an alkaline media and sufficient temperature any geologically derived material that is rich in aluminosilicate can produce a geopolymer (Yeddula & Karthiyaini, 2020a). Initially produced geopolymers uses, SiO_2 rich basic materials such as metakaolin (Venkatesh & Shanmugasundaram, 2024), but nowadays geopolymers are frequently made with industrial waste and byproducts (Meshram et al., 2024). Davidovits used the term "geopolymer" in 1988 to describe a binder in which silica (SiO_2) and alumina (Al_2O_3)-rich pozzolanic minerals, activated with an alkali solution, partially or completely replace OPC (Davidovits, 1988).

Subsequently, Davidovits (1994) described geopolymerization as the formation of an Al-O-Si bond through the reaction of aluminosilicate materials with alkali polysilicates. Since then, geopolymer composites have emerged as sustainable substitutes for cementitious materials based on OPC (Davidovits, 1994). ASTM states that when silica, calcium, alumina, magnesia and iron build up to a concentration of more than 70 % are classified as pozzolanic materials. These components are also present in GGBS in amounts higher than 70 % (Nicula et al., 2023). Through the utilization of industrial waste such as blast furnace slag, fly ash and metakaolin, geopolymer technology reduces CO_2 emissions (Wang & Ma, 2024) and dependency on carbon-intensive OPC while minimizing waste and conserving natural resources (Amari et al., 2024). Since geopolymers use industrial waste as their principal source, they have the potential to reduce these environmental issues (Konduru, Karthiyaini & Shanmugasundaram, 2025).

The practical application of RM requires high temperature activation, purification and neutralization treatment. Accelerated carbonation curing has significant potential for modifying industrial waste into suitable supplementary cementitious materials by reducing their alkalinity (Zhang et al., 2025d). The pH levels of RM can drop from 12 to 6.81 after carbonation (Mudgal et al., 2021a) and its alkalinity is decreased to limit the detrimental impact on the environment and to make its use as building material safer (Ilahi et al., 2024). The duration of Six days of CO_2 curing improves formation of carbonate phases inside the concrete matrix, enhancing the material's strength and characteristics (Saranya, Karthiyaini & Stone, 2025). Carbonation treatment can alter

the pore structure and surface reactivity by producing carbonate phases on the particle surfaces (Liu et al., 2021).

Notably, the carbonation of slag has a hydration-retarding impact in alkali-activated systems, in contrast to the hydration-promoting effect observed in ordinary cement systems. According to earlier research, the development of an amorphous carbonate layer on the slag surface prevents direct contact between the alkali activator and slag particles, and reduces the dissolution of ions such as Ca, Si and Al, thereby delaying setting (Cao et al., 2026). In dry carbonation of artificial aggregates made up of 50 % recycled concrete powder (RCP) and 50 % GGBS, involves exposing dried aggregates to high-purity CO_2 to promote gas-solid reactions with $Ca(OH)_2$ resulting in forming of $CaCO_3$, whereas wet carbonation involves immersing aggregates in CO_2-rich alkaline solutions, where CO_2 dissolves to form HCO_3^- ions, facilitating the reaction with Ca^{2+}. Additionally, wet carbonation produces well-crystallized calcite, which has a superior pore-filling capacity and greatly enhances aggregate compactness and mechanical performance (Zhang et al., 2025b).

Carbonation may also help immobilize heavy metals such as Cd, Zn, Pb, Cu and Cr that leach from alkaline solid waste (Pan et al., 2015). Red mud, hinders strength growth by interfering with hydration because of its high alkalinity and Na^+ concentration, which prevents stable binding gels formation and encourages competing carbonation processes. Granulated blast furnace slag increases the formation of C-A-S-H gel and supplies Ca^{2+} ions for carbonation. However, over time, microstructural densification increases the compressive strength while reducing CO_2 diffusion (Zhang et al., 2025e). The CO_2 curing of alkali activated binders is governed by the binder composition, curing conditions and type of alkali activator. The glass phase of Blast Furnace Slag (BFS) is more beneficial for carbonation reactions because of its CaO content (Jun, Han & Kim, 2024).

The majority of previous studies on RM-GGBS based geopolymer systems have concentrated on ambient or thermal curing, highlighting strength development, radiological safety, and basic microstructural characteristics. On the other hand, carbonation-induced phase evolution and its quantitative evaluation using methods like thermogravimetric analysis (TGA) have received relatively less attention.

This study explores the carbonation behaviour and CO_2 sequestration potential of RM-GGBS based geopolymer binders under varying alkaline molarities, with an emphasis on linking phase evolution, microstructure and mechanical performance. Unlike earlier studies that largely concentrate on either ambient or thermal curing conditions, the present study adopts a combined qualitative and quantitative approach to evaluate carbonation using SEM, XRD, and thermogravimetric analysis (TGA). The results indicate a composition driven trade-off between CO_2 uptake and strength development in RM-GGBS binder systems. Overall, this integrated assessment offers meaningful insights for carbonation characteristics of these binders and highlights the influence of mix composition on their microstructural and mechanical response.

The main objectives of the study are as follows:

1. The effect of carbonation curing on the mechanical performance of RM-GGBS based geopolymers was investigated.
2. The impact of mix composition and molarity under ambient and carbonation curing conditions was observed.
3. The phase formation and microstructural characteristics were examined using XRD and SEM analyses.
4. This study investigated how gel phases and calcite formation affected strength behaviour.
5. The carbon sequestration capacity of the binder material was evaluated using thermogravimetric analysis (TGA).

2. Materials, experimental methods and carbonation reaction mechanism

2.1. Raw materials

GGBS and RM were used as aluminosilicate precursors. To produce the alkali activator solution, sodium hydroxide pellets were dissolved in water to obtain a sodium hydroxide solution, which was then mixed with sodium silicate solution in proportions to reach the required molarity ratios of 2 Molar (2M), 4 Molar (4M), 6 Molar (6M) and 8 Molar (8M). Previous studies have examined the impact of sodium hydroxide concentration in the range of 4 to10 weight percent or approximately 1 - 2.5M, and have shown significant effects on compressive strength, as 54.43 MPa in weight percent of 8 (2M) of geopolymer systems (Liang & Ji, 2021). In comparison, the present study adopted a wider molarity range (2M–8M) to further explore the influence of alkaline activation under moderate to high concentration conditions. Red mud-based geopolymers have reportedly shown compressive strengths of 15.2 MPa at 2.5M NaOH and 20.3 MPa at 3.5M NaOH, indicating that improved dissolution, gel formation and mechanical performance require higher alkali molarities (Nie et al., 2016). It has been demonstrated that raising the NaOH concentration in carbonated red mud-based geopolymer systems from 0.5M to 2M increases compressive strength by encouraging geopolymerization and decreasing porosity; with the formation of well-developed N-A-S-H gel matrix at 2M results in the greatest strength (Mariyappan & Somasundaram, 2025). It has been reported that low molarity geopolymer systems (4M - 6M) can achieve compressive strengths of up to 40 MPa, demonstrating the viability of reduced alkaline concentrations for sustainable construction (Kumar et al., 2023a).

The chemical compositions of GGBS and red mud were determined by X-ray Fluorescence (XRF), and the results are presented in Table 1. The chemical compositions of GGBS and red mud mainly consist of Al_2O_3, Fe_2O_3, SiO_2, CaO and MgO. GGBS was procured from Astrra Chemicals, Chennai and red mud was sourced from an aluminium refinery in India.

Table 1. Oxide compositions of raw materials

Composition (wt %)	Al_2O_3	Fe_2O_3	SiO_2	TiO_2	CaO	MgO
Red mud	35.14	29.73	19.27	5.541	2.325	0.942
GGBS	23.81	0.3286	35.83	0.277	24.38	12.89

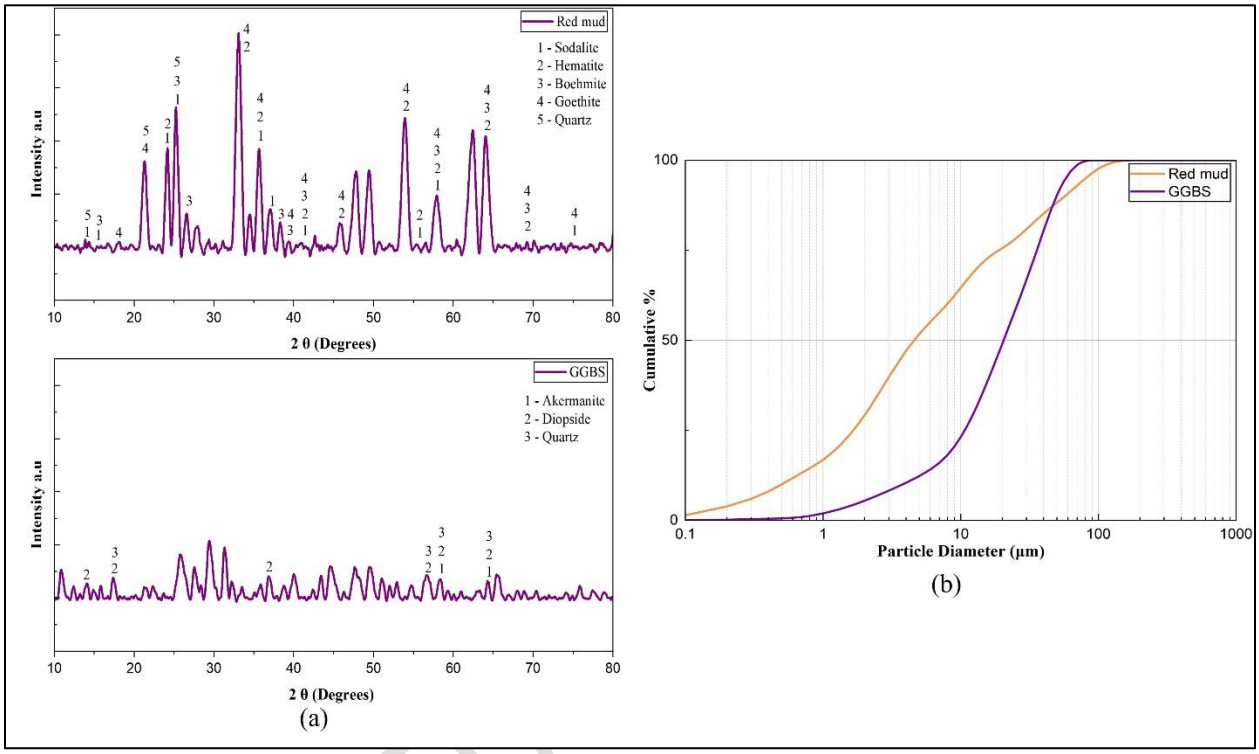

Figure 1. (a) XRD pattern of raw materials; (b) Particle size distribution of raw materials

Due to their high alkalinity and widespread production in worldwide these materials can be ideal feedstocks for CO_2 sequestration. Table 1 identifies Al_2O_3, Fe_2O_3 and SiO_2 as main constituents of RM with corresponding contents of 35.14 %, 29.73 % and 19.27 % and GGBS primarily comprises of Al_2O_3, SiO_2 and CaO with contents of 23.81 %, 35.83 % and 24.38 % respectively. The XRD pattern of raw materials depicted in **Figure 1a**. The main mineral phases in RM include boemite, goethite, hematite and sodalite. The Na_2 presence in RM may have contributed to create an alkaline environment to certain extent and favours faster dissolution (Yeddula & Karthiyaini, 2020b), even RM acts as a precursor. GGBS is predominantly composed of amorphous silicate minerals. The crystalline phases of GGBS consisted of an akermanite, diopside and quartz. The broad diffuse peaks shown in its XRD spectra, ensures that the material is in amorphous nature. This noteworthy combination of RM and GGBS has provided abundant Ca, Si, and Al elements as precursors, which have played a key role in subsequent chemical reaction process (Gao et al., 2025). The Laser Diffraction Particle Size Analyzer facility (CILAS-1180) from the National Centre for Earth Science Studies, Thiruvananthapuram was used to measure the particle size of raw materials. RM and GGBS has a mean diameter of 17.17 µm and

24.37 µm respectively. The results are depicted through particle size distribution curve illustrated in **Figure 1b**. while the characteristics of the particle sizes d90, d50, and d10 along their associated mean values are listed in Table 2.

Table 2. Particle size of ingredients

Diameter in Percentage	Red mud	GGBS
Diameter at 10 %	0.50 µm	3.78 µm
Diameter at 50 %	36.23 µm	20.48 µm
Diameter at 90 %	88.87 µm	49.62 µm

2.2. Sample preparation and carbonation unit

The aluminosilicate precursors used in this study were GGBS and RM. RM was employed as powdered form, without any further pre-treatment. Due to the finer particle size, the reactive surface area of the particle is increased, which results in more involvement in reactions (Wang, Kim & Qin, 2024). Previous studies indicated that pretreatment of raw materials are not necessary for mean particle size lesser that 100 µm (Polettini, Pomi & Stramazzo, 2016). The overall carbonation efficiency improved through uniform and effective chemical reactions due to their finer particle size (Saranya, Karthiyaini & Stone, 2025). A mixture of sodium hydroxide (NaOH) and sodium silicate (Na_2SiO_3) solutions used as an alkaline activator. The molarity of NaOH was set at 2 Molar (2M), 4 Molar (4M), 6 Molar (6M) and 8 Molar (8M), while maintaining a Na_2SiO_3 to NaOH weight ratio of 2:1. For complete dissolution and temperature stabilization NaOH solutions were prepared 24 hours prior to mixing. Geopolymer paste mixtures were developed using six different proportions of RM and GGBS with weight ratios of 100:0, 80:20, 60:40, 40:60, 20:80 and 0:100 across all molarities. Since different red mud and GGBS contents have been shown to have a significant impact on the dissolution behavior, gel formation, and mechanical performance of alkali-activated systems, the RM:GGBS ratios (100:0 to 0:100) were chosen to systematically investigate the influence of precursor composition on geopolymerization (Jin et al., 2024). A constant solid to liquid ratio of 0.5 was maintained, consistent with ratio adopted for this work. Previous studies have reported that a liquid-to-solid ratio as 0.55, provides an optimal balance between workability and mechanical performance in geopolymer systems, enabling adequate flowability for casting while maintaining strength development (Qingke et al., 2024). Based on this, a solid-to-liquid ratio of 0.5 was adopted in the present study to ensure sufficient workability. The components were mixed manually by hand until a consistent paste was formed. The paste was then poured into cylindrical moulds with dimensions 32.5 mm in diameter and 65 mm in height. Two curing methods were applied namely Carbonation Curing (CC) and Ambient Curing (AM). In carbonation curing moulds filled with fresh geopolymer paste were placed promptly inside the carbonation curing unit for six days and once cured the specimens were removed from the curing unit and kept exposed to air, then tested at 28 days to evaluate the compressive strength. Previous findings have shown that carbonation behaviour in alkali-activated systems is strongly influenced by CO_2 curing conditions such as pressure, concentration and

temperature, which significantly affect microstructure and mechanical performance (Sun et al., 2025). Therefore, controlled CO_2 curing parameters were adopted in the present study to ensure effective carbonation and consistent reaction conditions. The CO_2 gas was periodically replenished at a constant supply pressure of 50 kg/cm^2 to maintain the saturation level inside the carbonation curing unit (Chandralega & Shanmugasundaram, 2026), (Venkatachalam & Somasundaram, 2026). Additionally, CO_2 replenishment was done to maintain a stable CO_2 environment within the curing system and to make up for gas consumption during the reaction, guaranteeing consistent microstructural growth and prolonged carbonation kinetics (Chandralega, Shanmugasundaram & Stone, 2025). The temperature and relative humidity (RH) were controlled at 30 ± 2 ºC and 85 ± 5 % respectively inside the carbonation unit during curing. The samples underwent six days curing to investigate the effects of the binder in the CO_2 exposure. As the curing age of carbonation increased, which results in longer diffusion path for CO_2 for participating in the chemical reaction, leading reduced rate of carbonation. Hence, carbonation triggered by CO_2 curing via chemical reactions between Carbon dioxide, water and dissolved ions in the matrix (Mohamed et al., 2024).

2.3. Carbonation reaction mechanism

Nowadays the CO_2 curing method progressively brought forward for preparation and curing of concrete products (Liu & Li, 2023). In calcium-based cement system such as ordinary Portland cement (OPC), carbonation curing induces the reaction of CO_2 with calcium silicates to form calcium carbonate and CSH gel, resulting in strength improvement by matrix densification (Thonemann et al., 2022). Similarly, in calcium-based geopolymer system, carbonation curing triggers the reaction of CO_2 with calcium aluminosilicates to form calcium carbonate and C-A-S-H gel, thereby better strength development and matrix densification can obtain. Carbonation curing technology is effectively reducing carbon emissions while enhancing the density and mechanical properties (Lyu et al., 2024). The carbonation reaction mechanism encompasses multi-phase reaction mechanism of aqueous carbonation like gas-liquid phase and liquid-solid phase. The general carbonation reaction equation is demonstrated in **Figure 2a** and carbonation curing unit is shown in **Figure 2b**. The carbonation reaction process can be explained as follows. The gaseous CO_2 (g) was turned into aqueous CO_2 (aq) when diffuses into binder sample (Kurusta et al., 2023). The CO_2 (aq), combines with water present in the binder, then form carbonic acid (H_2CO_3) (aq). Generated carbonic acid dissociates to produce bicarbonate (HCO_3^-) (aq), carbonate (CO_3^{2-}) (aq) and some hydrogen ions (H^+) (Kurusta et al., 2023; Kahyarian, Brown & Nesic, n.d.). In previous study of steel slag reported the promotion of carbonic anhydrase, enhance the CO_2 hydration and facilitates to combine with Ca^{2+} (Luo & He, 2021). Likewise, this may influence the Ca^{2+} ions present in the precursor material associate with carbonates and form as $CaCO_3$ (s) within the matrix. The CO_2 addition functions similar to an admixture addition, in that it reacts with calcium ions from hydrated cement to alter the concrete's state into a solid state, generating $CaCO_3$ as the solid CO_2 sequestered inside the matrix without leaving any gas leftovers (Ahmed, Ahmad & Adekunle, 2024).

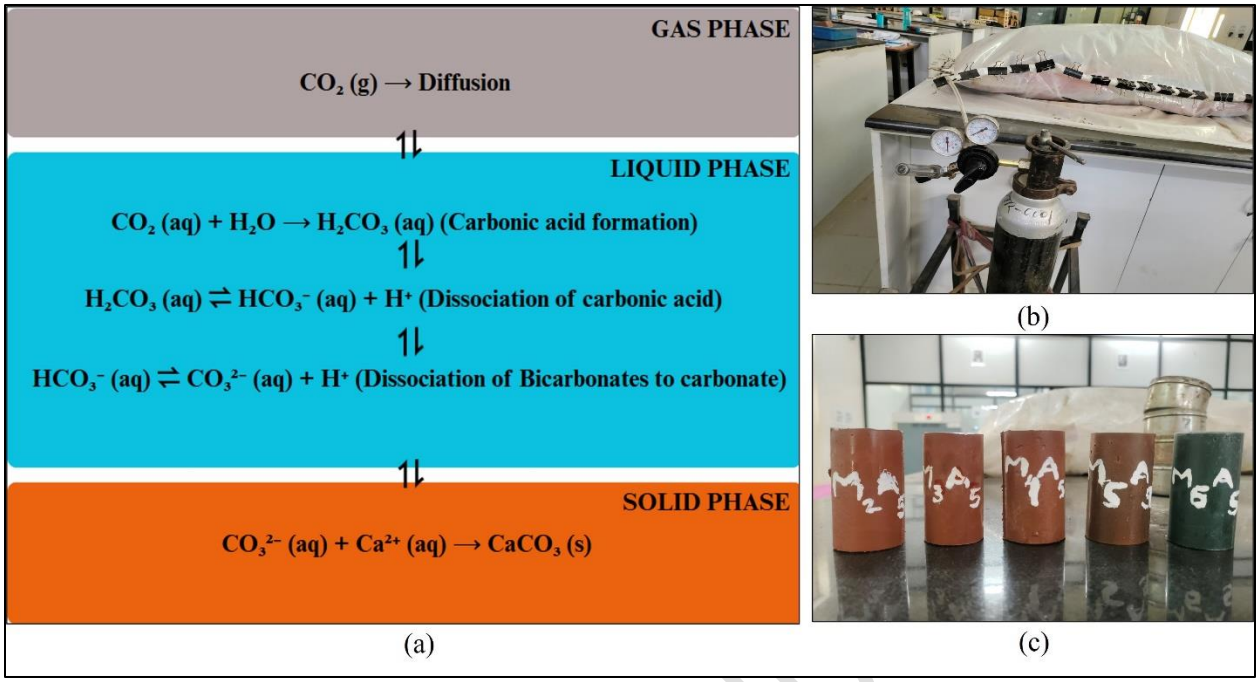

Figure 2. (a) Carbonation reaction process; (b) Carbonation curing unit; (c) Ambient cured samples.

2.4. Compressive strength

The physico mechanical performance of the geopolymer specimens were evaluated by conducting compressive strength test. The cylinders casted with a diameter of 32.5 mm diameter and height of 65 mm were assessed using a Compressive Testing Machine (CTM-SHIMADZU, Concreto 2000X) with a maximum capacity of 2000 KN, according to the procedures specified in IS 516 (2021) (Standard, 2021). The cylindrical specimens were loaded until they fractured at a rate of 0.5 MPa/s. The average strength of each geopolymer mix was determined by testing three specimens of each mixture.

2.5. Microstructural (SEM-EDS) and Phase (XRD) characterization of geopolymer samples

The morphology of ambient cured and carbonation cured samples was examined using high-resolution scanning electron microscopy (SEM). The 5000x magnification was used for both ambient cured and carbonation cured samples. The crystalline phases of the raw materials, ambient cured and carbonation cured hardened samples were identified using XRD analysis. The powdered samples were prepared using an agate mortar and pestle and then the samples were analyzed using CuK radiation operated at 40 kV and 40 mA with scanning carried out over a 2θ range from 5º to 80º.

2.6. Thermogravimetric Analysis (TGA)

TGA was performed on samples prepared for XRD and SEM analyses. The samples were tested using a Hitachi 7200. The temperature range was 30 - 900 ºC, and the heating rate was 15 ºC/min under a nitrogen atmosphere. The TG and DTG curves were plotted for each sample.

Table 3. Mix designation of geopolymer samples.

Molarity	Mix Designation		Composition (Weight Percentage)
	Ambient Curing	Carbonation Curing	RM: GGBS
2M	AC2MM1	-	100:0
	AC2MM2	CC2MM2	80:20
	AC2MM3	CC2MM3	60:40
	AC2MM4	CC2MM4	40:60
	AC2MM5	CC2MM5	20:80
	AC2MM6	CC2MM6	0:100
4M	AC4MM1	-	100:0
	AC4MM2	CC4MM2	80:20
	AC4MM3	CC4MM3	60:40
	AC4MM4	CC4MM4	40:60
	AC4MM5	CC4MM5	20:80
	AC4MM6	CC4MM6	0:100
6M	AC6MM1	-	100:0
	AC6MM2	CC6MM2	80:20
	AC6MM3	CC6MM3	60:40
	AC6MM4	CC6MM4	40:60
	AC6MM5	CC6MM5	20:80
	AC6MM6	CC6MM6	0:100
8M	AC8MM1	-	100:0
	AC8MM2	CC8MM2	80:20
	AC8MM3	CC8MM3	60:40
	AC8MM4	CC8MM4	40:60
	AC8MM5	CC8MM5	20:80
	AC8MM6	CC8MM6	0:100

Note: AC stands for Ambient Curing and CC stands for Carbonation Curing. M1, M2, M3, M4, M5 and M6 are mix ID's.

3. Results and Discussion

3.1. Compressive strength of Geopolymer samples

The geopolymer samples of 2M, 4M, 6M and 8M were tested for compressive strength at the age of 28 days, as shown in **Figure 3**. A gradual increase in the compressive strength was observed as the GGBS content increases. Previous studies have reported that the inclusion of GGBS in FA-based geopolymer mortar results in increased strength, demonstrating the positive

effect of GGBS content on mechanical performance (J & P R, 2024). The mix designations with molarity and curing are depicted in Table 3. The lowest strength (13.24 MPa) was recorded at AC2MM2, whereas the highest strength (52.48 MPa) was achieved at AC2MM6 (GGBS-based) in the 2M ambient cured samples. The excess RM content could be the cause of the decline in compressive strength. When RM content exceeded 30%, which prevents geopolymerization process by increasing the undissolved phases, thereby increasing the crystalline content (Simha, Yeddula & Somasundaram, 2020). The strength development in geopolymer composites is ascribed to the formation of N-A-S-H and C-A-S-H gels. The incorporation of red mud can impede the development of C-A-S-H gel and hence decrease the compressive strength of the geopolymer (Li et al., 2023). For the 6M ambient cured samples, the lowest and highest strengths were recorded as 9.01 MPa and 27.96 MPa, respectively.

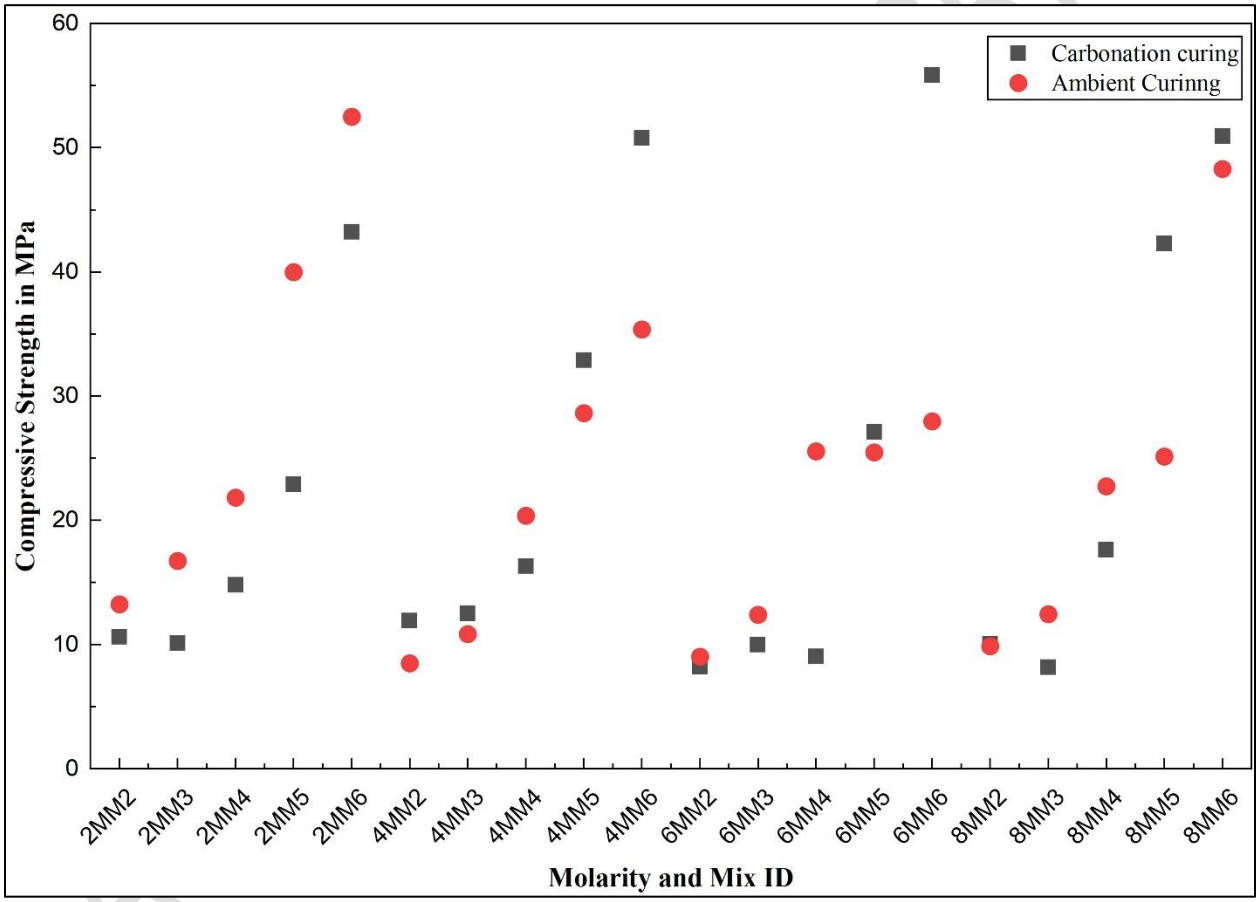

Figure 3. Compressive strength of carbonation cured and ambient cured geopolymer samples. 2M, 4M, 6M and 8M denotes molarities: M2, M3, M4, M5 and M6 denotes mix ID's

On the other hand, 2M carbonated cured samples resulted lower compressive strength as 10.01 MPa and highest strength as 43.22 MPa, whereas 6M samples played a significant role as lowest strength as 8.2 MPa and highest strength as 55.81 MPa. The GGBS-based samples revealed ideal performance, while partial replacement of RM up to 20 - 40% maintains moderate strength. This demonstrates that the capability of red mud as a supplementary material without fully

compromising the strength gain in ambient curing. In RM-based binary geopolymer synthesis, the author concluded that the compressive strength achieved as 27.2 MPa by incorporating RM at 50% (Hao et al., 2025). The development stays same in all the molarities of the geopolymer concrete mix developed. Notably, the mixes activated with 2M NaOH solution exhibited higher compressive strength than those with 4M, 6M and 8M, especially in GGBS-rich compositions under ambient curing. This trend deviates from the common report of increase in strength with rising molarity. By the results, it suggests that the strength would not always follow higher molarity, especially under ambient curing. In ambient cured samples 2M NaOH outperformed while comparing with 4M, 6M and 8M, indicating better balanced reaction environment at lower molarity may have allowed for better microstructural development in the GGBS-rich mixes. Meanwhile the GGBS-based 4M and 6M NaOH results in rather low compressive strength as 35.36 MPa and 27.96 MPa when compare to 2M and 8M in ambient cured samples. The studies have also indicated that still achieve compressive strength ranges from 10 - 40 MPa under ambient curing with low molarity like 4M and 6M (Kumar et al., 2023b). In carbonated samples 6M NaOH performed better than other molarities as high compressive strength of 55.81 MPa. The geopolymer strength increased with lesser amount of RM content in all curing ages. The surplus amount of RM cause structural degradation with reduced compressive strength of geopolymer (An et al., 2022).

The comparison of compressive strength of the geopolymer samples based on the curing regime were illustrated in **Figure 4**. Across all the molarities (2M, 4M, 6M & 8M) the M1 mix displayed very low compressive strength due to high workability, so it was excluded from the further work. In previous findings also the author identified that the compressive strength of 100% RM as 0.5 MPa and revealed that as evidence for RM-based geopolymers is in need of supplementary source to improve their strength (Mishra et al., 2024a). For each molarity the samples exhibit low strength (LS) and high strength (HS) under each curing regimes were compared to show strength variation. Samples under CC2MM3 presents comparatively low strength in carbonated cured sample by 24.40% when compared to the ambient cured sample. The decrease of compressive strength with increasing red mud due to formation of zeolite minerals. Increasing amount of red mud beyond 15% of weight causes decrease of compressive strength (Mudgal et al., 2021b). Under a fixed solid-to-liquid ratio of 0.5, the proportion of red mud (RM) to ground granulated blast furnace slag (GGBS) is anticipated to significantly influence paste flowability. This is due to the relatively porous and water-absorbing nature of red mud, in contrast to GGBS, which generally enhances particle packing and rheological response (Sun, M & Saji, 2026) (Kanyal, Agrawal & Gupta, 2021). Previous research has demonstrated that increasing the GGBS content can decrease yield stress and plastic viscosity, thereby enhancing flowability (Akhlaq et al., 2025). Conversely, the incorporation of red mud may alter workability due to its fine particle characteristics and water demand. The higher RM content may prolong the setting time and decrease the viscosity and thixotropy of slag-based geopolymers which also leads to a decrease in mechanical strength (Li et al., 2021). However, differences in workability may influence the compactness of the hardened matrix of all mixes examined in this study. The

observed differences in compressive strength are considered to be governed primarily by the extent of geopolymerization process (Li et al., 2021) rather than solely to workability.

The AC2MM6 samples demonstrates high strength in ambient curing, whereas carbonated samples display rather lesser about 17.6% relative to the compressive strength of ambient cured sample of 52.48 MPa. On the other hand, ambient cured samples show low and high compressive strength for 6M specimens ranging from 9.01 to 27.96 MPa, while the carbonated cured samples display from 8.2 to 55.81 MPa. The reduction of RM content, results in increased compressive strength of the RM-GGBS based geopolymers. On account of greater reactive potential, GGBS granting quicker dissolution behaviour, which enabling early development of geopolymer network and resulting high early strength, irrespective of alkaline concentration (Zakira et al., 2023)**.** The strength of the geopolymer ascribed to the formation of N-A-S-H and C-A-S-H gels resulting in the formation of three-dimensional network by condensation process. GGBS specifically triggers the reaction of aluminosilicate hydrates and the formation of hydration products due to its elevated CaO content, which could expedite the setting reaction of geopolymers (Yang et al., 2025). Among all four molarities and both curing methods the 4M and 8M samples represents intermediate compressive strengths. The 4M ambient cured samples resulted 8.49 MPa as low compressive strength and 35.36 MPa as higher compressive strength when carbonated curing highlights low compressive strength as 11.92 MPa and 50.77 MPa as higher compressive strength. In contrast 8M samples achieved lower and upper bounds of compressive strength measured at 9.86 and 48.28 MPa respectively in ambient curing, whereas carbonated curing recorded as 8.15 and 50.91 MPa in that order.

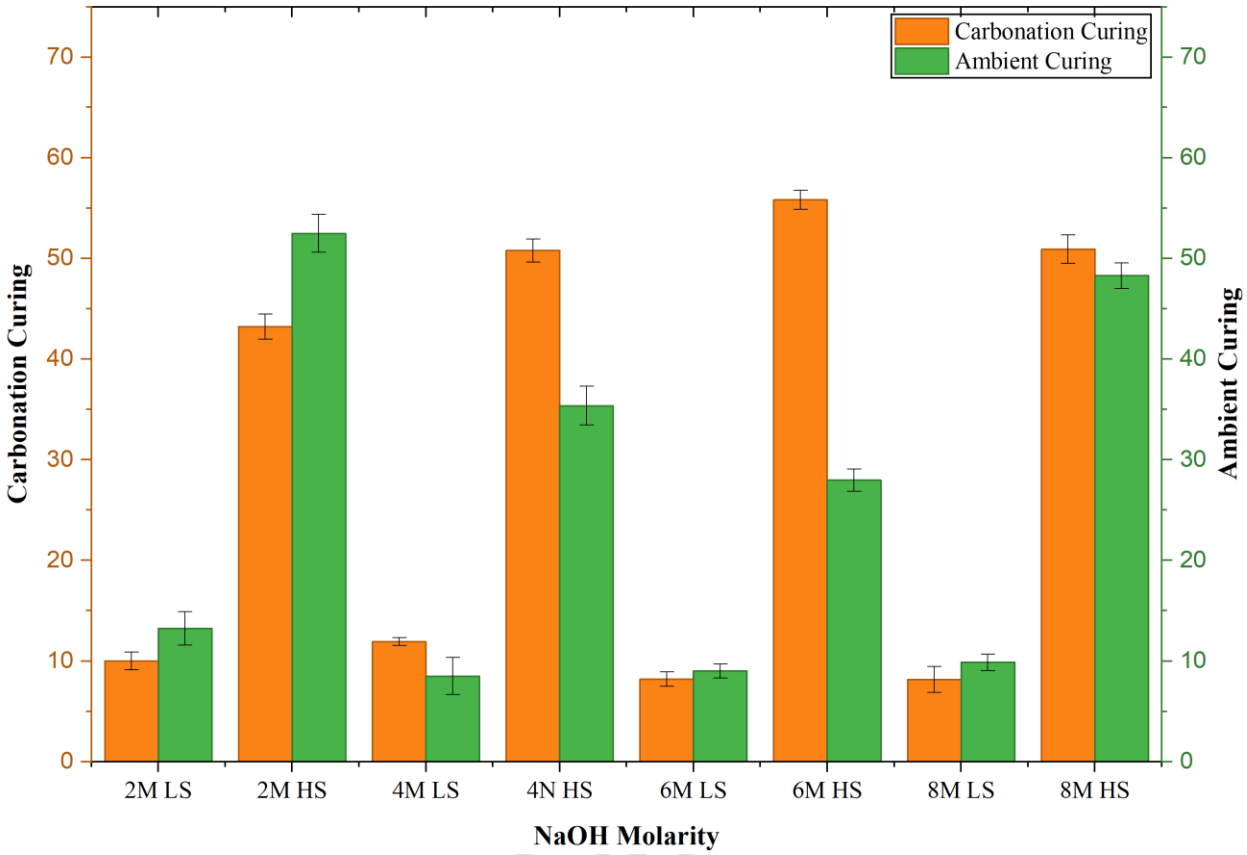

Figure 4. Comparison of low-strength (LS) and high-strength (HS) of geopolymer samples in terms of compressive strength (MPa) based on NaOH molarity and curing

3.2. XRD analysis of geopolymer samples

The XRD patterns of the carbonation cured samples are shown in **Figure 5**. In the carbonation curing of 2M samples, the XRD spectra displayed alite, calcite, hematite and quartz as unreacted phases. A substantial increase in the calcite peak intensity indicates, that the carbonation process improves $CaCO_3$ deposition, thereby filling the pores of the geopolymer paste and densifying the structure (Venkatachalam & Somasundaram, 2026). The increased intensity of the calcite peak confirms the effective carbonation of calcium hydroxide, which simultaneously produces partial decalcification of C-S-H gels (Zhang et al., 2025c). Although the calcite formation

densifies the matrix, the impact of hematite promotes decomposition of alite which

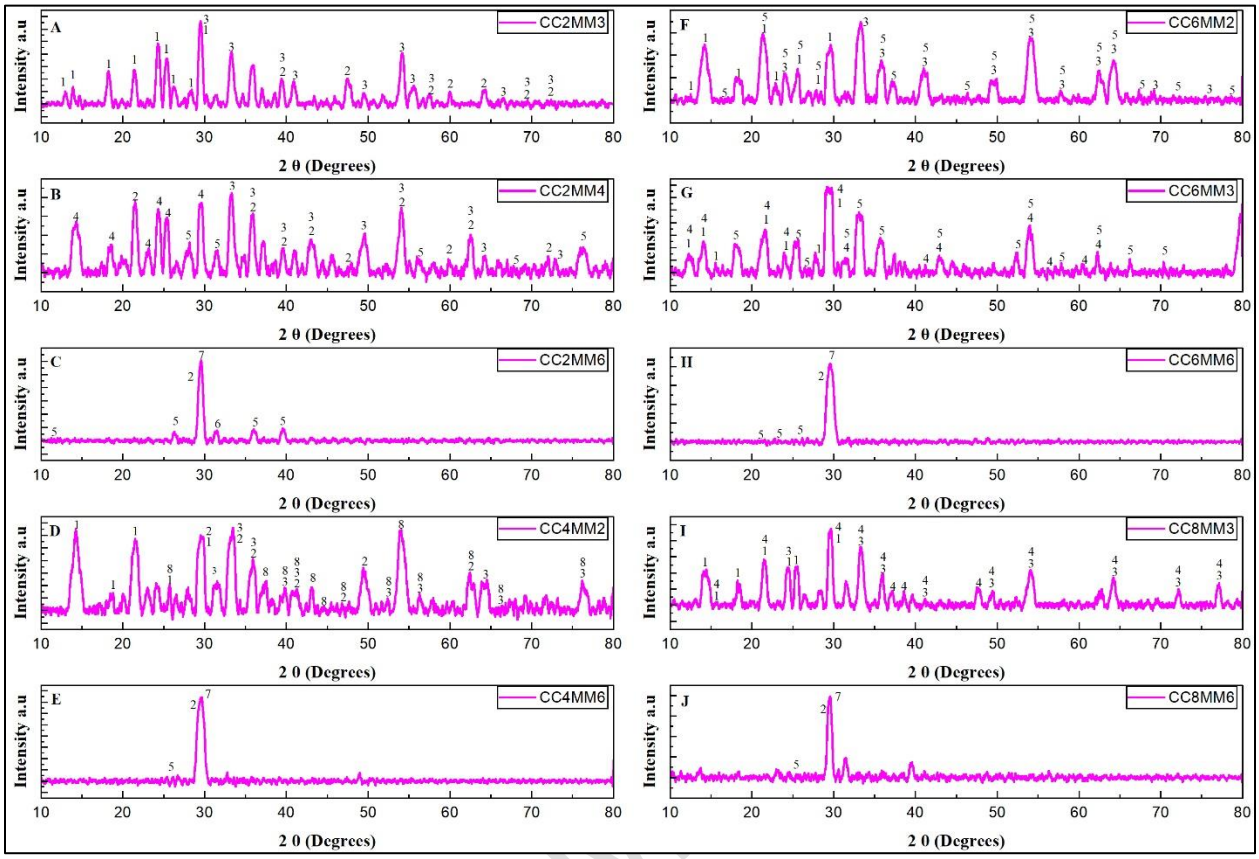

Figure 5. XRD patterns of carbonation cured samples (1:Alite, 2:Calcite, 3:Hematite, 4:N-A-S-H, 5:Quartz, 6:Thermonatrite, 7:C-A-S-H, 8:Titanium oxide)

produces CSH that contributes the most to strength, and thereby reduces (Zayed et al., 2020). Hematite and quartz were specifically generated from the raw materials and persisted after 28-day hydration pointing their poor reactivity within the alkaline conditions. The existence of Na^{+} and OH^{-} ions increases the dissolution of precursor materials and encourages polymerization with Al^{3+}, Si^{4+} and Ca^{2+} ions, resulting in the formation of C-S-H, C-A-S-H and N-A-S-H. These gels are the chief contributors to strength development in geopolymers. These phases are reflected as amorphous diffraction peaks between 22º and 38º (Liu et al., 2024a). The XRD spectra confirmed that N-A-S-H was the dominant phase owing to the alkali activation of aluminosilicates. Furthermore, the existence of NaOH in the alkaline solution improved the progress of the amorphous N-A-S-H gels. This process leads to better mechanical strength and chemical durability of the geopolymer concrete (H M & M S, 2025). In the present study, the formation of thermonatrite was observed in CC2MM6 as a secondary phase of the main geopolymer matrix. This is noticeable when alkali activated binders are exposed to CO_2 rich environments leads to the formation of hydrated and anhydrous sodium carbonates: in particular thermonatrite can form if the pH of the pore solution is high (Moro et al., 2021). Calcium sources present in the geopolymer matrix, linked to the generation of C-A-S-H gel, develop hydration reactions such as setting,

hardening and prolonged strength development of the material (H.M. & Unnikrishnan, 2023). The 4M and 8M carbonated samples resulted in low strength as the red mud content increased up to 60% due to the formation of inert crystalline phases like hematite, which did not dissolve and remained just as fillers (Ai et al., 2021; Koshy et al., 2019).

The performance of ambient cured geopolymer specimen's XRD spectra illustrated in **Figure 6**. and the ambient cured samples are depicted in **Figure 2c**. Variation in phase composition was noted across all four molarities of samples like cancrinite, hematite, quartz, N-A-S-H and C-A-S-H. An observed phase transition of cancrinite mostly happened due to the presence of Na_2CO_3 in the specimen, which promote the sodalite to cancrinite transformation (Vogrin et al., 2020). Out of the formed phases cancrinite, hematite and quartz were derived by the raw materials, and the existence of those phases after 28-days hydration indicates their inert behaviour under alkaline condition (Li et al., 2025b). N-A-S-H gel formed in AC2MM4 could play main role in this geopolymer paste for strength gain when compare to AC2MM2. The N-A-S-H formation may serve a key responsibility in the geopolymer strength gain and C-A-S-H have a relatively low significance here (Uysal et al., 2024). AC2MM6 out performed well among other samples. XRD spectra revealed crystalline phases of quartz, C-A-S-H and N-A-S-H gels together displayed the strength development. The calcium content present in the GGBS encourages the generation of C-A-S-H and it acted as nucleation site. Within the system it encouraging the occurrence of suitable alkali activators (A. & O.M., 2024). All the blends indicated the presence of cancrinite, hematite and quartz phases in its XRD pattern of RM-rich mixes (AC2MM2, AC2MM4, AC4MM2, AC6MM2 and AC8MM2). When the molarity increases in this mix it shows some N-A-S-H gel phases in its XRD spectra. According to Davidovits, ambient cured geopolymers are generally amorphous with some non-crystalline phases, inclusion of quartz, muscovite or hematite, rely on the precursor used. This is attributed by the presence of halo shaped peaks in the range between 20 - 30º in 2θ instead of sharp crystalline peaks due to lowest percentage of GGBS. This shape may be originated from unreacted precursors (Amar et al., 2024). But in the present study muscovite minerals have not formed. AC4MM6 shown quartz and C-A-S-H gel formation. Gel formation is attributed to the availability of reactive calcium and silicate species. Earlier studies reported that the formation of C-A-H phases while employing 100% GGBS as the precursor materials (Li et al., 2025a). The 6M based ambient cured samples of AC6MM2, AC6MM5 and AC6MM6 have displayed hematite, quartz, N-A-S-H and C-A-S-H in its XRD spectra. Hematite

presence partially dissolved in alkaline environment and primarily form $NaFeO_2$, thereby influence

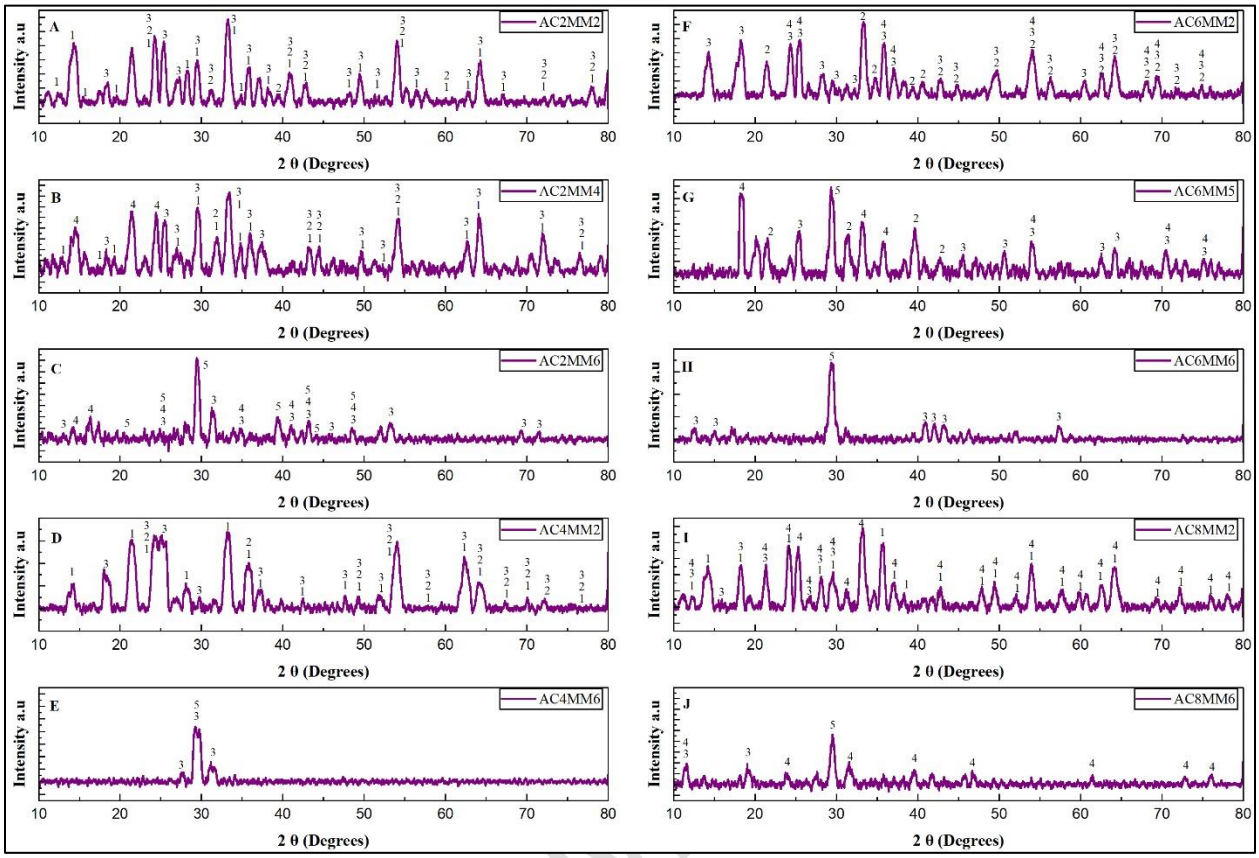

Figure 6. XRD pattern of ambient cured samples (1:Cancrinite, 2:Hematite, 3:Quartz, 4:N-A-S-H, 5:C-A-S-H)

the degree of polymerization and pore structure, resulted in considerable changes in compressive strength of samples (Wu et al., 2024). Excess hematite presence in samples indicated high percentage of unreacted red mud (Anon, 2025). Based on the observation of AC6MM6, it demonstrated quartz and C-A-S-H phase formation. In high calcium slag-based system silicates undergoes further depolymerization due to the high CaO content (Lang et al., 2025). This may be the reason of development of low strength in this system. According to the observation of AC8MM2 samples, it revealed combined appearance of both N-A-S-H and C-A-S-H gels. Low calcium system like RM-based geopolymer, main reaction product is generation of N-A-S-H gel and hence relatively loose small gel pores are formed (Osio-Norgaard, Gevaudan & Srubar, 2018). This may be the reason for reduced strength of AC8MM2 about 9.85 MPa. The AC8MM6 reported quartz, N-A-S-H and C-A-S-H gel phases in its XRD pattern. N-A-S-H gel formation in this GGBS-based samples, may due to the higher molarity concentration. The high concentration of NaOH molarity involved in the formation of N-A-S-H gel by denser microstructure development (Shamsah, Kalfat & Subramaniam, 2025) and hence resulted in better strength development. In all GGBS-rich samples there is a formation of C-A-S-H in peaks. The solubility and reaction degree of activators significantly interrupted by Na_2CO_3 then it is influencing the reaction kinetics of

$Ca(OH)_2$. There is no residual formation of $Ca(OH)_2$ peaks, indicating that $Ca(OH)_2$ contributed to the formation of C-A-S-H gel (Guo et al., 2026). The comparative analysis of the peak intensities across the ambient and carbonated samples confirms the significant impact of curing conditions and activator molarity on the geopolymerization and carbonation products. The quantitative data confirms a substantial increase in Calcite ($CaCO_3$) formation at approximately 29.4º, 2theta following carbonation curing. In the 2M system, the calcite peak intensity surged from 14.94 units in the ambient sample, AC2MM2 to 33.17 units in the carbonated sample, CC2MM3. A similar trend is observed in the 6M and 8M systems. For instance, CC2MM6 exhibited a calcite intensity of 30.26 units, more than double that of its ambient counterpart AC2MM6 with 14.41 units. This quantitative leap supports the qualitative observation that carbonation curing effectively facilitates $CaCO_3$ deposition within the matrix, which leads to the densification of the microstructure and the filling of capillary pores. The data reveals a clear reduction in the intensity of Alite (C_3S) peaks near 32.5º of 2θ in carbonated samples, indicating its consumption during the carbonation process. For the AC2MM2 sample, the Alite peak intensity was recorded at 22.19 units, which significantly dropped to 12.45 units in CC2MM3. This consumption is attributed to the accelerated decomposition of alite in the presence of CO_2, which contributes to the formation of additional C-S-H and subsequent calcite. Similarly, Hematite (Fe_2O_3) intensities at 33.1º in 2theta remained relatively high in samples containing a higher percentage of red mud (RM). The AC2MM2 and AC6MM2 showed intensities of 29.29 and 25.99 units, respectively. In carbonated samples like CC2MM3 having 20.99 units and CC6MM2 having 17.41 units, the hematite persists, confirming its role as a predominantly unreacted phase that serves as a micro-filler but can hinder the reactivity of other phases if present in excess. The formation of amorphous gels is evidenced by the broad hump in the 20º to 35º of 2θ range. Quantitative assessment of the average intensity in this region shows higher values for GGBS-rich samples and those with higher molarity. In the AC8MM2 sample, which recorded a strength of 9.85 MPa, the presence of both N-A-S-H and C-A-S-H was supported by a stable intensity baseline. The AC8MM6 sample showed a distinct quartz intensity of 1.07 units and an average hump intensity that suggests a denser N-A-S-H framework. The increase in NaOH molarity corresponds to higher dissolution of precursors, as seen in the slightly lower intensities of unreacted quartz in high-molarity samples compared to low-molarity ones, like Quartz intensity in AC2MM2 was 8.01 against 1.07 in AC8MM6. The detection of Thermonatrite ($Na_2CO_3.H_2O$) around 32.2º, 2θ is more pronounced in the carbonated series. In the 6M samples, CC6MM2 and CC6MM3, intensities reached 7.41 and 5.99 units, respectively. This quantitative presence indicates that some of the sodium from the activator reacted with the diffused CO_2, forming sodium carbonates. The absence of $Ca(OH)_2$ peaks, Portlandite in the quantitative data across all samples suggests that the calcium provided by the GGBS was entirely consumed in the formation of C-A-S-H gels or calcite.

3.3. Characterization geopolymer samples using SEM with image analysis

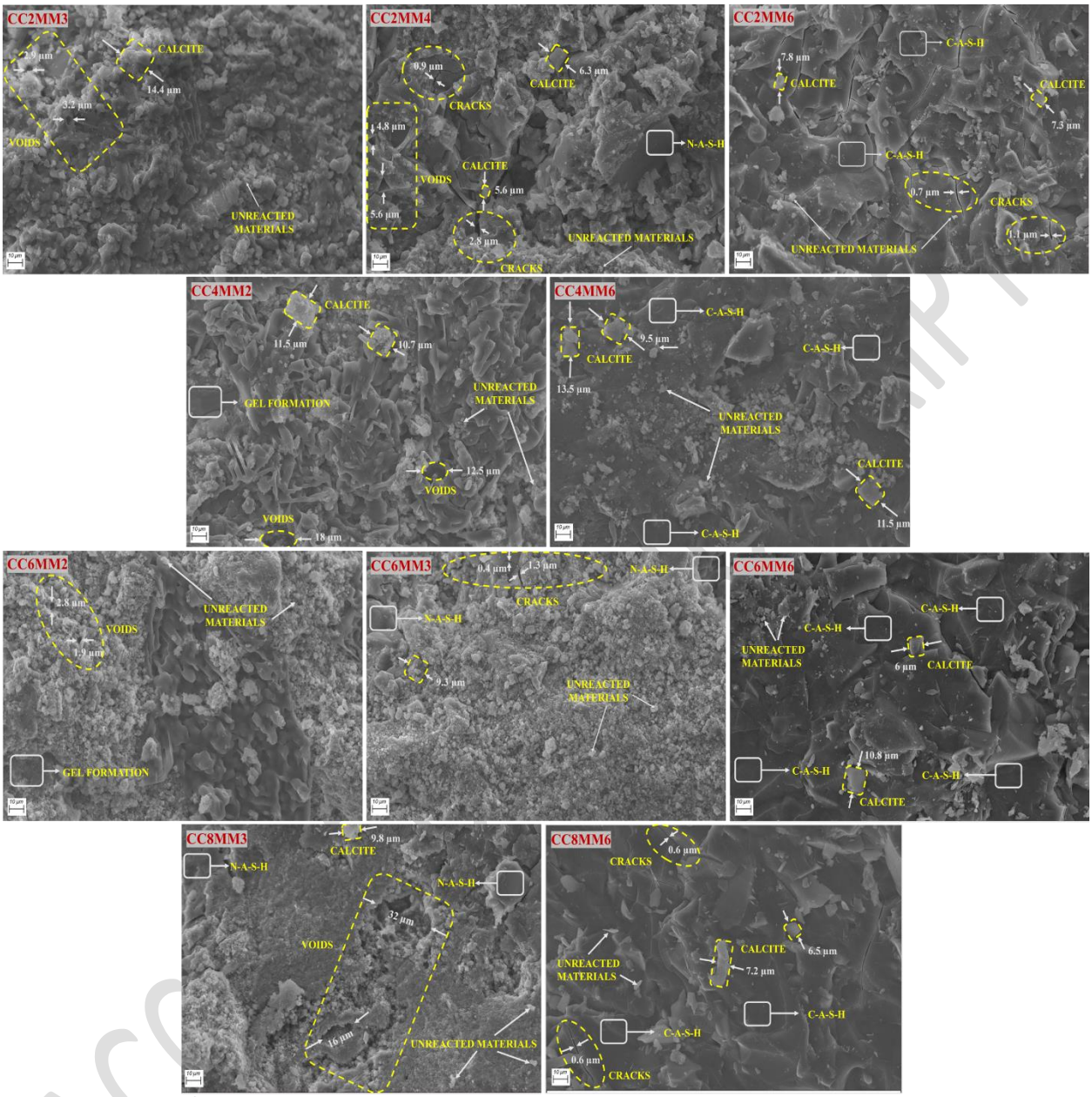

Figure 7. SEM images of Carbonation cured samples with image analysis

SEM analysis was used to investigate the morphological characteristics of the carbonation cured and ambient cured samples derived from RM and GGBS, as shown in **Figure 7** and **Figure 8** respectively. The microstructural phases showed the reaction mechanisms that occurred within the binder including voids, cracks, unreacted materials, amorphous gel and crystalline phases. Geopolymer gels appeared in some samples with few partially reacted phases. A decrease in compressive strength was observed in samples with higher RM content, thereby increasing the

number and size of voids. The loose porous structure of RM influences its porosity and water absorption when incorporated into a binder system (Peng et al., 2025).

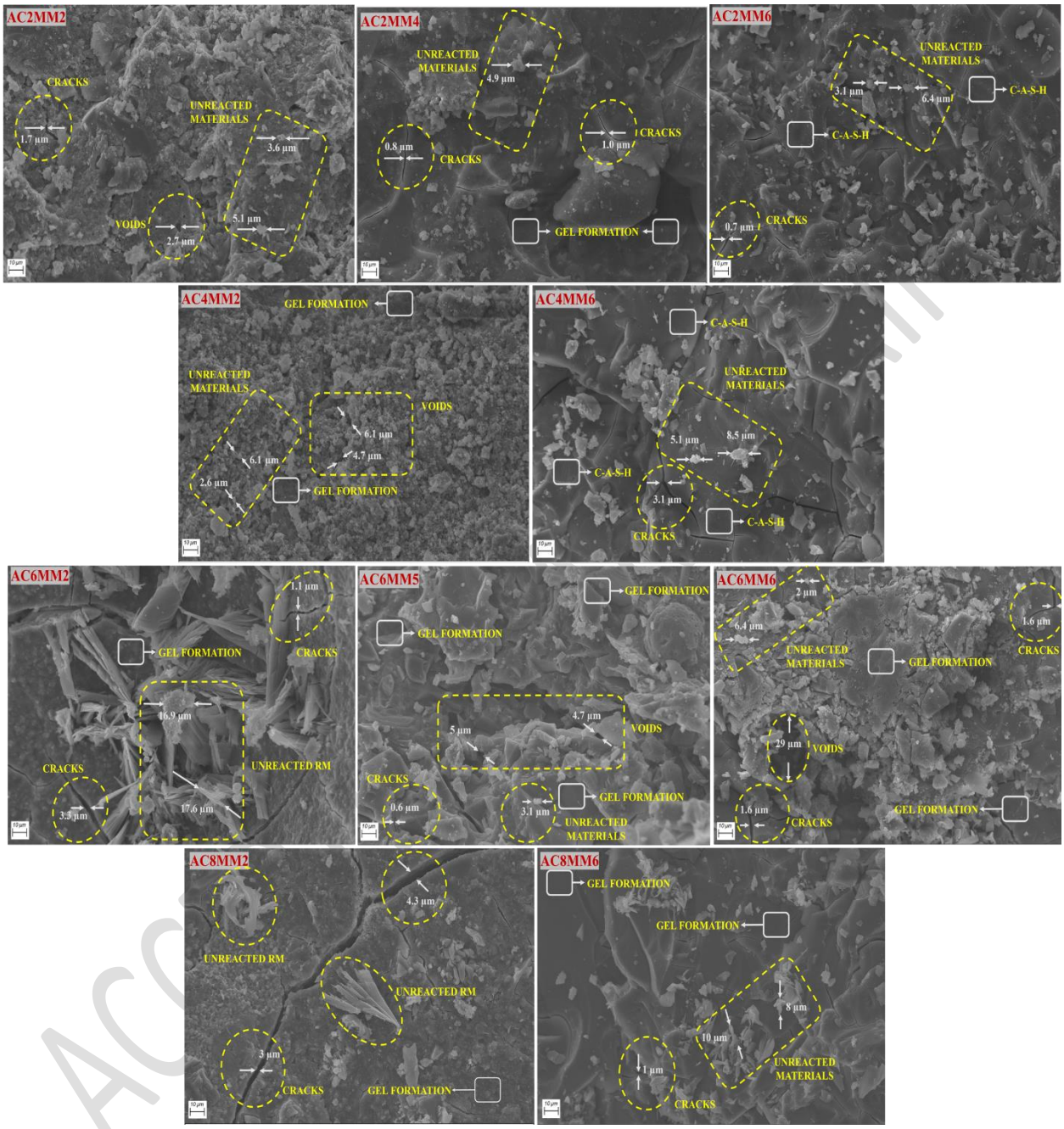

Figure 8. SEM images of Ambient Cured samples with image analysis

The hardened specimen of CC2MM3 particles persisted with smooth edges and noticeable agglomeration and there was no evident of formation of hydration products. So that it indicates hydration degree of RM is limited. The availability of reactive Ca and Si phases controls the synthesis of common hydration products such as C-S-H and $Ca(OH)_2$, suggesting a limited degree of hydration (Zhu et al., 2023). Aluminosilicate gels are formed in AC6MM2 with glassy

microstructure, in contrast to angular crystalline particles with more cracks. Highly agglomerated hematite particles were observed in SEM morphology. The location of such phases confirms strong consistent Fe and O signals with a hematite composition. However, excessive hematite has a physical encapsulating effect on the hydration products, delaying their early-stage hydration reactions. Excessive hematite simultaneously forms hematite interfaces that prevent later-stage hydration products from bonding (Wu et al., 2025).

It can be observed that most of the samples with 100 % GGBS solidified by reacting well with the alkaline solution and had a dense matrix structure of carbonated samples, whereas some ambient cured samples had air voids and cracks. The increase in GGBS content enhanced the reaction with the alkali solution and liberated large amount of heat to form more C-A-S-H, resulting in overall strength development (Fahim Huseien et al., 2017). Across all 100 % GGBS mixes, the carbonated curing improved the performance of all samples except CC2MM6 specimen, where thermonatrite formation reduced the strength and multiple cracks spotted in its SEM image. This phase causes inner crystallization pressure within the binder gel, which weakens the matrix, and hence the mechanical strength is reduced (Firdous et al., 2021).

Among the two specimens with identical molarity of 6 and mixed composition (M6), the carbonated cured sample exhibited better performance, and the densification effect of carbonation is responsible for this improvement, which increases matrix compactness and decreases porosity (Beltrame et al., 2023). Whereas ambient cured sample spotted multiple cracks and voids in its SEM image. However, in ambient curing the binders produced from 100 % GGBS tend to exhibit greater shrinkage and formation of micro cracks, which hinders the overall performance (Mishra et al., 2024b). According to the calcium content present in the precursor, the specimen AC6MM5 and AC6MM6 showed more gel formation in their SEM images, with persistent pores and cracks. The N-A-S-H gel formation may occur because of the high molarity of the mix. Hence, sufficient alkali and aluminosilicates are available from RM, to support the better but significant synthesis of the N-A-S-H gel. In addition, the presence of unreacted material may decrease the matrix integrity, which may cause the reduction in strength and performance. This reduction is due to the effect of unreactivity and proportionally shows its impact on the formation of voids with a more porous micro structure with higher embedded micro cracks. The observed porous and cracked microstructure, along with the presence of unreacted particles, indicates incomplete geopolymerization (Mohammed, Singh & Fanijo, 2025), leading to reduced matrix integrity and increased void formation.

The SEM image further confirms the micro structural variations induced by the curing conditions in AC2MM4 and CC2MM4. The combination of C-A-S-H and N-A-S-H gel formation with some unreacted ferrite phases and calcite was observed in the SEM images. A well-developed gel phase identified in AC2MM4, may be due to the presence of Ca rich phases forming robust C-A-S-H and hybrid gels compared to CC2MM4. These hybrid gel systems have been extensively documented in calcium-containing geopolymer matrices and are associated with improved microstructural performance and compactness. The interaction of Ca^{2+} with dissolved silicate and

aluminate species in these hybrid gel systems is known to enhance matrix densification and compactness (Ganesan & Ravichandran, 2026). The gel chemistry was similar for both specimens. However, in the carbonation cured sample, the C-A-S-H gel can be decalcified due to leaching of alkalis while forming as carbonate crystals and reducing the connectivity in the matrix. The existence of N-A-S-H after carbonation may cause porosity and result in a loss of mechanical strength. Previous findings of fly ash-based control samples exhibited a gel structure of C-(N)-A-S-H with the accumulation of unreacted fly ash particles and microcracks, resulting in a heterogeneous micro structure (Tran et al., 2024).

3.3.1. SEM-EDS Analysis

An EDS full area analysis was performed for all specimens to further determine the type and amount of geopolymer gel generated. The results are presented in **Table 4 and Table 5**. The results demonstrate that the major elements are Ca, Na, Al, Si and O, suggesting possible formation of geopolymer reaction product in the RM-GGBS based geopolymer paste. The amount of geopolymer gel generated in each mix was identified by Ca/Si, Na/Si and Si/Al ratio. Based on the elemental ratios, the reaction products may be associated with C-A-S-H, N-A-S-H and C-(N)-A-S-H type gels. No clear boundary was observed between these gels; instead, they were interwoven to form a continuous geopolymer matrix across the scanned area (Bai et al., 2024).

Table 4. The atomic percentage of different elements of carbonation cured samples

Mix ID	Na	Al	Si	Ca	C	O	Ca/Si	Na/Si	Si/Al
CC2MM3	14.0	0.8	1.6	0.6	24.8	57.0	0.38	8.75	2.0
CC2MM4	3.4	2.9	2.9	1.4	15.6	49.7	0.48	1.17	1.0
CC2MM6	3.8	3.4	8.4	8.8	15.3	57.5	1.05	0.45	2.47
CC4MM2	12.9	0.8	1.4	2.8	21.4	56.4	2.0	9.21	1.75
CC4MM6	8.6	1.9	5.8	6.2	17.9	58.3	1.07	1.48	3.05
CC6MM2	12.5	1.9	2.0	0.5	23.5	57.1	0.25	6.25	1.05
CC6MM3	5.9	3.5	8.9	3.1	14.2	60.3	0.35	0.66	2.54
CC6MM6	3.5	2.7	6.9	8.6	18.0	57.8	1.25	0.51	2.55
CC8MM3	2.2	9.3	1.8	1.4	22.4	52.3	0.78	1.22	0.19
CC8MM6	3.7	3.1	7.6	7.6	16.9	59.2	1.0	0.49	2.45

Table 5. The atomic percentage of different elements of ambient cured samples

Mix ID	Na	Al	Si	Ca	C	O	Ca/Si	Na/Si	Si/Al
AC2MM2	5.5	2.9	4.2	0.6	20.1	46.9	0.14	1.31	1.45
AC2MM4	5.3	4.3	4.8	3.9	20.4	56.2	0.81	1.10	1.12
AC2MM6	6.1	2.8	7.0	7.1	17.0	57.5	1.01	0.87	2.5
AC4MM2	4.6	10.3	2.0	1.6	23.0	54.7	0.80	2.30	0.19
AC4MM6	4.6	3.3	9.5	9.8	18.2	51.3	1.03	0.48	2.88
AC6MM2	1.1	12.6	0.7	0.1	19.5	63.4	0.14	1.57	0.06
AC6MM5	4.6	2.5	5.8	7.1	26.7	49.3	1.22	0.79	0.43
AC6MM6	5.3	3.0	7.4	8.4	16.6	56.9	1.14	0.72	2.47
AC8MM2	4.0	1.6	2.0	0.8	15.7	48.7	0.4	2.0	1.25

AC8MM6	10.1	1.4	3.2	6.4	23.1	54.2	2.0	3.16	2.29

As shown in **Table 4** and **Table 5** the GGBS-rich mix (M6) displayed significantly higher Ca and Si contents, consistent with the chemistry of GGBS. The elevated Ca concentration suggest the formation of Ca-rich binding gels, such as C-A-S-H, which are responsible for the enhanced mechanical properties of slag-based alkali-activated systems. Furthermore, the Ca/Si and Si/Al ratios from 1 to 2 and 2.29 to 3.05, respectively suggests the possible formation of C-A-S-H in GGBS-rich specimens under both carbonation and ambient curing. Previous findings have shown that higher Ca/Si and Si/Al ratios in C-A-S-H gel typically correspond to a highly cross-linked three-dimensional structure. Therefore, the increased Si/Al ratio may have contributed to promote the polymerization degree of the C-A-S-H gel network, leading to a denser microstructure and enhancing the compressive strength (Vashistha, Oinam & Pyo, 2023). Higher Si/Al ratios promote greater polymerization and mechanical integrity, whereas lower ratios improve thermal resistance (Vignesh, Ramesh & Xavier, 2025).

The Na/Si ratio indicates the influence of alkali content, where higher values promote precursor dissolution and gel formation, though excessive alkalinity may affect matrix densification and transport properties. The production of SiO_4 and AlO_4 tetrahedra as well as a dense three-dimensional network is encouraged by the increased dissolution of precursors with increasing Na_2O, content due to increased alkalinity. However, excessive Na_2O makes the solution more viscous, which limits ion mobility and prevents further dissolution, ultimately weakening the microstructure (Sasui et al., 2024). RM-rich mixes (M2, M3, M4 and M5) revealed higher Na/Si ratio when compare the 100 % GGBS mix (M6). Carbonation curing causes microcracking, which is associated with the quick breakdown of reaction products and possible shrinkage. The rapid decalcification of the C-A-S-H gel may cause reduction in the Ca/Si ratio, which was verified by the EDS results (Yue, Dhandapani & Bernal, 2025).

3.4. Comparative discussion on Compressive Strength of geopolymer samples

The moderate strength gain caused by better geopolymerization observed in some mixes of RM-GGBS based geopolymers under ambient curing. The alkaline solution promotes dissolution of aluminosilicates and calcium phases from red mud and GGBS respectively, resulting in the appearance of composite gel matrix of N-A-S-H and C-A-S-H gels. According to earlier research, aluminosilicate-rich precursors promote the synthesis of N-A-S-H gel, but GGBS provides the Ca^{2+} required for C-A-S-H formation, allowing hybrid gel structures to form under ambient curing conditions (Ganesan & Ravichandran, 2026). These combined gel phases result in a denser matrix and better structural integrity. This study reported that ambient cured RM-GGBS based geopolymers achieve compressive strengths ranging between 8.49 - 25.46 MPa at 28 days in M2, M3, M4 and M5. Based on the alkaline activator combination and composition of precursor materials both N-A-S-H and C-A-S-H gel can form in association within the matrix. The noted improvements in compressive strength have been observed in the presence of slag most likely results in the formation of calcium-based gel structure along with N-A-S-H leads to denser and more compact micro structure (Ozcelikci et al., 2023). In previous study that showed clearly that

the GGBS-based systems gain strength irrespective of activator molarity, an account of their calcium-rich composition priorly and the continuous C-A-S-H gel formation even at low molarities (Nguyen, Goodier & Austin, 2020). Thereby the C-A-S-H gel enhances binding and reduces capillary porosity.

In carbonation-cured specimens, it has been observed that the trend of compressive strength reduction in RM-rich mixes (M2, M3 and M4). This characterization may be the result of decalcification of C-A-S-H gels caused by the reaction of carbonates with Ca^{2+} ions, resulting in $CaCO_3$ precipitation. However, the initial stage carbonation can densify the matrix through filling the pores, the prolonged exposure cause reduction in gel continuity as consumption of calcium. Because of this ongoing exposure, carbonation cured RM-GGBS based samples typically exhibits the compressive strength of 8.2 to 14.8 MPa, which are roughly 3 to 45 % lower than ambient-cured specimens in the mixture of M2, M3, M4 and M5. This drop in strength could be caused by calcite formation, which could impair the inter-gel bond between the calcium and aluminosilicate phases and disturb the geopolymer framework. In cases of excessive carbonation, partial decalcification and disruption of the gel network may occur, leading to a reduction in structural integrity. Since RM is a low Ca precursor, it creates faster decline of pH than precursors rich in CaO (Lamaa et al., 2023). This is due to the formation of thermonatrite during the carbonation of Na^+ ions owing to incomplete dissolution of precursors in NaOH (Werling et al., 2020) and thereby inhibiting the dissolution of aluminosilicates and the polymerization of N-A-S-H gel. The accelerated carbonation process caused the primary binding phase, an aluminium-substituted calcium silicate hydrate (C-(N)-A-S-H) gel, to lose calcium, leading to the production of calcium carbonate.(Bernal, 2016). In ternary blended RM-GGBS based geopolymers, CO_3^{2-} in the solution inhibits the dissolution of RM and GGBS by modifying alkalinity and forming $CaCO_3$, prior of C-A-S-H gel formation, during initial activation of RM with Na_2CO_3 (Li et al., 2025c). An increase in sodium hydroxide solution concentration improves the dissolution of sodium silicate and aluminium phases of GGBS into the solution and accelerates geopolymerization (Kumar Poloju & Srinivasu, 2022). Thus the 100% GGBS specimens revealed better compressive strength as the molarity increases.

3.5. Comparative discussion on XRD Analysis of geopolymer samples

The XRD diffractogram of ambient-cured RM-GGBS geopolymers exhibited occasional crystalline peaks for unreacted phases such as cancrinite, hematite, and quartz along with consistent amorphous geopolymer gels like N-A-S-H and C-A-S-H in a large diffuse hump between 25º and 35º in 2θ. Furthermore, the presence of these crystalline phases contributes to the geopolymer-hardened matrix. Compared to carbonated curing, the spectra revealed no indication of calcite formation, and the amorphous halo reflected the major amorphous matrix of alkali-activated gel formation responsible for strength development. Structural changes such as low peak intensities and the development of an amorphous hump in the XRD spectra by visual inspection, indicate gel formation (Albayrak & Özen, 2025)

On the other hand, the carbonation-cured specimens considerably change the XRD pattern with a modified diffraction profile and developing calcite crystalline peaks, confirming CO_2 fixation within the matrix at characteristic 2θ values of 29.4º, 39.5º, 43.6º and 47.4º as a main product, which is consistent with previous findings (Harirchi & Yang, 2022). This shows that in alkali-activated systems, causes calcium leach from C-A-S-H gels and precipitation of carbonates when expose to carbonation. The prolonged exposure to carbonation showed stronger, sharper calcite peaks of stable calcite and resulting diminishing of amorphous halo. That is the decalcified C-A-S-H gel turns to a less-stable silica-rich N-A-S-H / C-(N)-A-S-H type hybrid gel, justifying lower strength performance after carbonation in RM-GGBS based geopolymer samples. In the previous study also confirmed that formation of calcite as a main crystalline phase, together with decrease in amorphous content, indicating transformation of gel structure post-carbonation (Albayrak & Özen 2025). But in GGBS based geopolymers that are M6 of all molarities revealed better C-A-S-H gel formation with minimum crystalline peaks in their XRD spectra. The previous findings revealed that increase in GGBS content improves the mechanical strength and gel formation observed in micrographs (H.M. & Unnikrishnan, 2023). GGBS promotes the formation of C-A-S-H gels by replacing Si in C-S-H gels with Al and hence increasing both quality and quantity of gels (Liu et al., 2024b).

3.6. Comparative discussion on SEM Morphology of geopolymer samples

The SEM micrographs support the above findings. The ambient-cured RM-GGBS geopolymer exhibited a continuous gel matrix with small cracks. SEM observations highlighted voids, unreacted particles and an integrated gel matrix. Although the RM-GGBS based specimens had some small cracks and voids, good strength was observed when compared with the carbonated cured specimens. The gel formation along with minerals originating from RM such as hematite and cancrinite, may combine to form a strong framework to provide higher mechanical strength (Raza et al., 2024). The 100 % GGBS samples at all molarities resulted in better gel formation in their SEM images, although they had some cracks and voids. The similarity exists in the previous findings of GGBS-based geopolymer cured at ambient condition, showed well distributed small pores in its gel phases and significant improvement in compressive strength was observed (Zhou et al., 2020).

The carbonated-cured RM-GGBS geopolymer exhibited regions of calcite, micro cracks, voids and still presence of unreacted materials along with geopolymer gels. Except 100 % GGBS mix at each molarity, gel formation of C-(N)-A-S-H or simply N-A-S-H gel formation appeared. The C-(N)-A-S-H gel might have caused an increase in voids due to its high molarity compared to the carbonation products (Azar et al., 2024). The GGBS-based carbonated samples showed cube shaped crystals or small particle like calcite in the SEM images. They were found to seal the surface pores of geopolymers with a spongy C-A-S-H gel matrix, resulting in a denser microstructure (Li & Ikeda, 2024). Similar morphological were observed in the present study for 100 % GGBS based geopolymer showing filling of voids and enhanced matrix densification.

3.7. TGA and CO_2 uptake

Figure 9 shows the results of the thermal analysis of ambient and carbonated cured RM-GGBS based geopolymer paste, where **Figure 9 (a) and 9 (b)** displays the TG and DTG curves of ambient cured samples and **Figure 9 (c) and 9 (d)** depicts the TG and DTG curves of carbonation cured samples. The CO_2 content can be calculated from the mass loss curve and the CO_2 uptake can be calculated based on the mass loss of the samples at temperatures ranging from 550 to 850 ºC, corresponding to decarbonation of $CaCO_3$. The residual mass at 850 ºC was selected, rather than the initial mass, to eliminate the confounding effects of moisture and volatiles, which do not contribute to carbonation. This approach quantifies CO_2 uptake in relation to the stable geopolymer matrix involved in the carbonation process. The CO_2 uptake (Zhao et al., 2025) was determined using the following formula.

$$CO_2 \text{ uptake} = [\Delta W_{(550\,^{\circ}C - 850\,^{\circ}C)} / W_{850\,^{\circ}C}] * 100\ \% \quad (1)$$

From **Figure 9 (b) and 9 (d),** it can be seen that four peaks existed in the DTG curve. The initial peak of about 150 ºC is attributed to the loss of physically bound water. The peak at 350 ºC is due to the dehydration of chemically bound water surrounded by alkali cations such as Na or K (Ettahiri et al., 2023). The mass loss occurred between 450 and 550 ºC was owing to dehydroxylation of portlandite phase as a minor loss (Sun et al., 2025). This study revealed that minimum portlandite formation, ascribed to low 2.325 % CaO presence in RM and approximately 25 % CaO in GGBS. Even though GGBS has more CaO, it consumed more for C-A-S-H gelation and the rest leaving trace free CH formation.

A distinct mass-loss occurred between 550 and 850 ºC ascribed to the decarbonation of calcite ($CaCO_3$) phase formed during CO_2 curing (Liu & Li, 2023). The mass loss peak shifted to the right as the carbonation increases in the RM-containing mixes, indicating a better crystallinity of calcite in these samples. The mass loss and CO_2 uptake of each sample are displayed in **Table 6.**

Table 6. Comparison of CO_2 sequestration capacity of RM-GGBS based geopolymer paste by ambient curing and carbonation curing

Mix ID	Mass loss (%)	CO_2 uptake (%)	Mix ID	Mass loss (%)	CO_2 uptake (%)
AC2MM2	1.8	2.3	CC2MM3	3.3	4.0
AC2MM4	2.5	3.2	CC2MM4	3.2	3.9
AC2MM6	2.9	4.0	CC2MM6	2.9	3.6
AC4MM2	3.1	4.2	CC4MM2	3.7	4.5
AC4MM6	1.8	2.4	CC4MM6	2.1	2.6
AC6MM2	3.0	4.1	CC6MM2	3.6	4.5
AC6MM5	2.1	2.8	CC6MM3	2.4	3.0
AC6MM6	1.2	1.5	CC6MM6	2.3	2.9
AC8MM2	1.1	1.4	CC8MM3	3.3	4.2
AC8MM6	1.6	2.1	CC8MM6	2.4	3.1

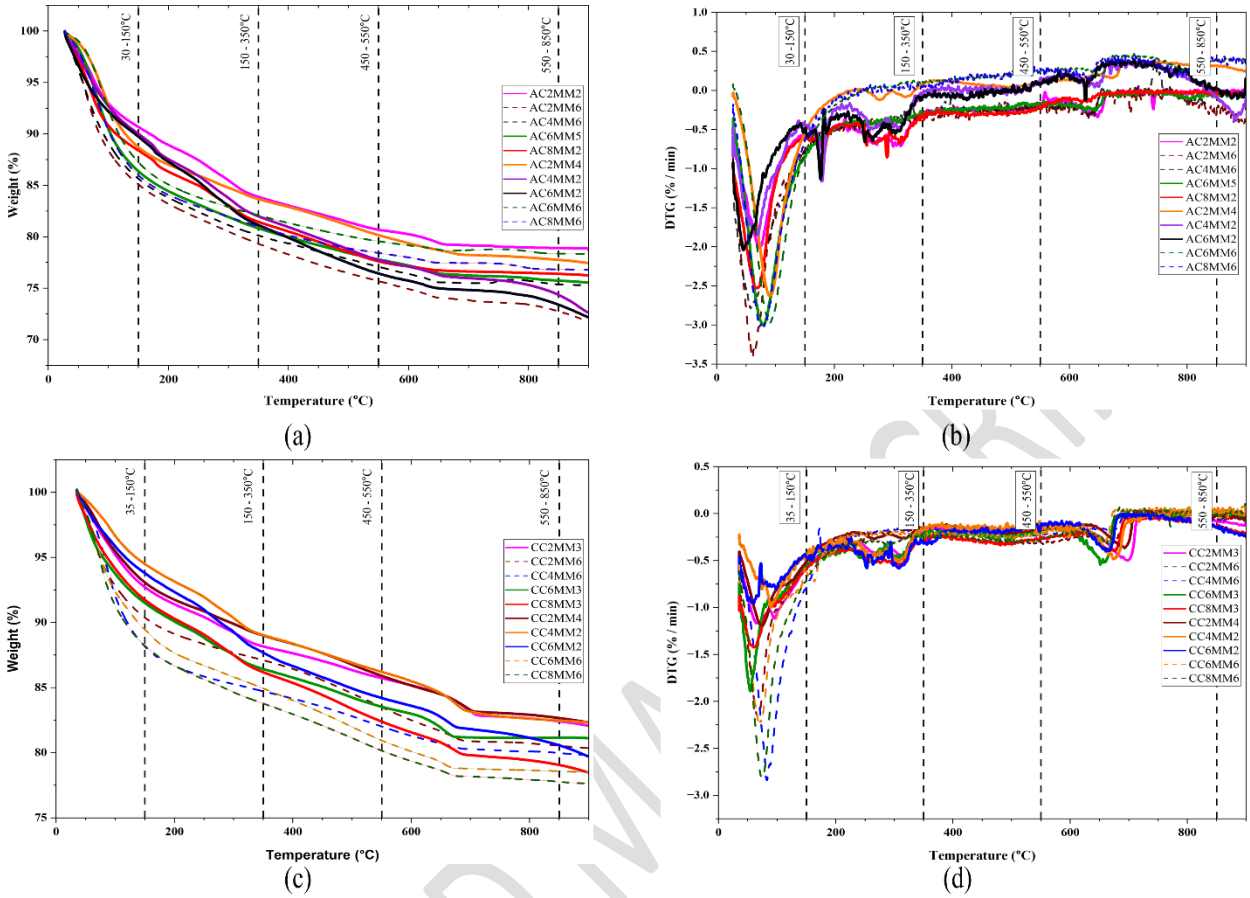

Figure 9. (a) TG Curve of ambient cured sample, (b) DTG curve of ambient cured samples, (c) TG curve of carbonation cured samples and (d) DTG curve of carbonation cured samples

In recent studies, carbon capture and storage (CCS) technology has been identified as a potential approach for lowering CO_2 emissions (Liu et al., 2022). A Comparison of CO_2 sequestration capacity of the RM-GGBS based geopolymer paste subjected to ambient and carbonation curing is presented in **Table 6**. The mass loss percentage of CO_2 content can be calculated directly from the TG curve using the following formula:

$$CO_2 \text{ content} = W_{550\,^{\circ}C} - W_{850\,^{\circ}C} \quad (2)$$

Where the CO_2 content is the mass loss of CO_2 bound in calcium carbonate, $W_{550\,^{\circ}C}$ is the mass loss at 550 ºC and $W_{850\,^{\circ}C}$ is the mass loss at 850 ºC. The **Figure 10** shows comparison of CO_2 uptake of various mix composition with molarity. The mass loss and CO_2 uptake results indicated a clear difference between the ambient and carbonation cured samples. Overall, carbonation cured samples exhibited higher mass loss and CO_2 uptake than ambient cured samples, confirming the effectiveness of carbonation curing in enhancing CO_2 sequestration. In the ambient cured samples, moderate CO_2 uptake was observed, with values generally increasing at lower

molarity levels (2M and 4M) and decreasing at higher molarities (6M and 8M). Early carbonation in the paste was encouraged by a less dense matrix with a lower activator concentration, which facilitated CO_2 diffusion (Jun, Han & Kim, 2023). Among these, mixes containing both RM and GGBS (M2, M3, M4 and M5) showed relatively better performance than the 100% GGBS mix (M6), indicating the beneficial role of RM in facilitating carbonation reactions under ambient conditions.

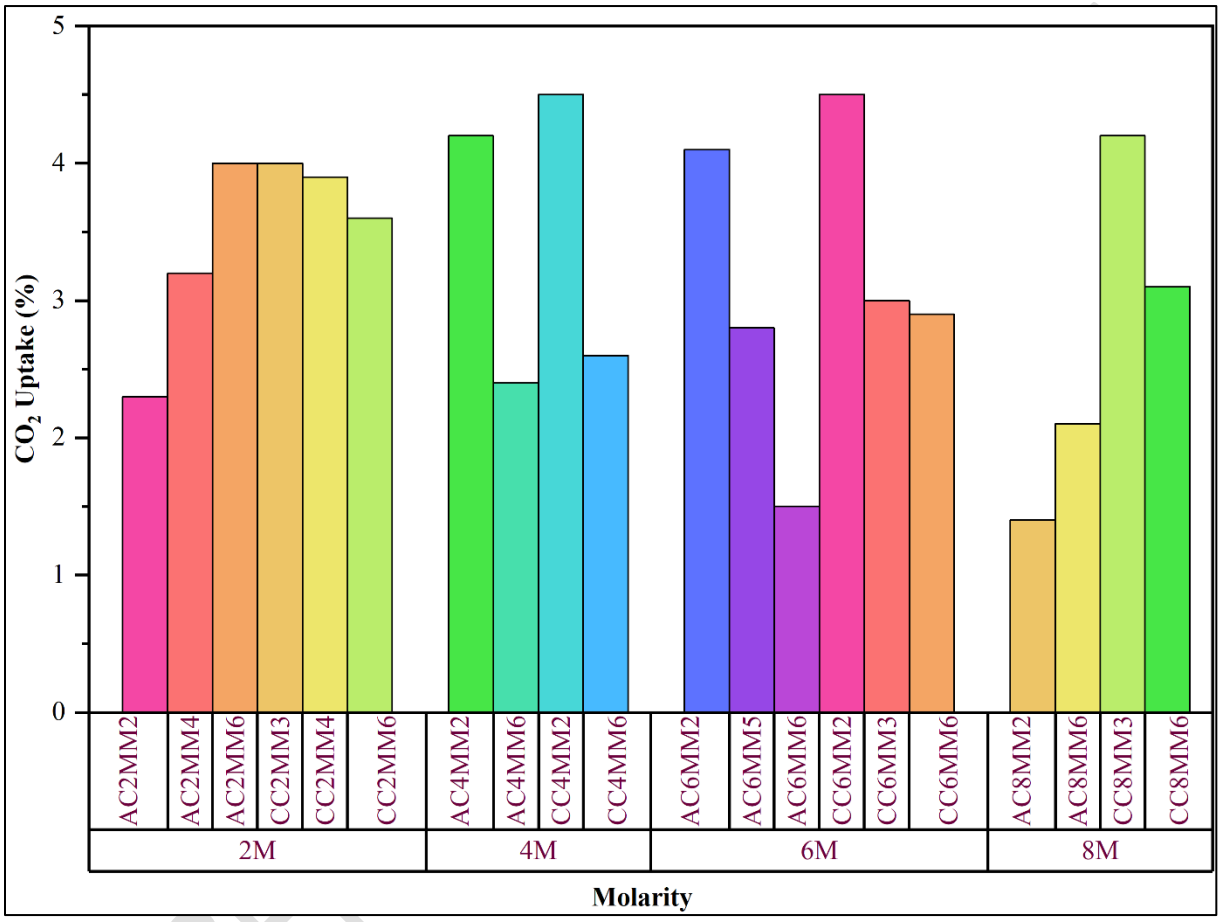

Figure 10. Comparison of CO_2 Uptake among various mix composition with molarity

In contrast, the carbonation-cured samples consistently demonstrated higher CO_2 uptake across all mixes. The RM-containing mixes (M2, M3, M4 and M5) again showed improved performance compared to the 100% GGBS mix (M6), suggesting that the presence of RM enhanced carbonate formation. RM has a high potential for efficiently absorbing mineralized CO_2 because of its small particle size, large pores and significant alkalinity, which create thermodynamically stable products during carbonation (Zhang et al., 2024).

However, in some higher molarity mixes, a slight reduction in CO_2 uptake was observed, possibly due to the densification of the matrix, which limits CO_2 diffusion. Even though alkalinity initially promotes dissolution, the simultaneous formation of reaction products consumes available alkalis and limits mass transport, thereby reducing the early-stage reaction kinetics in GBFS-MK

blends (Bernal et al., 2011). Overall, the results highlight that carbonation curing significantly improves CO_2 sequestration, and the incorporation of red mud further enhances this effect compared with pure GGBS systems.

4. Conclusions

The current study investigated the effect of curing regimes on the strength properties and micro structural performance of RM-GGBS based geopolymer paste through the evaluation of compressive strength, X-ray diffraction (XRD), scanning electron spectroscopy (SEM) and Thermogravimetric analysis (TGA). The following insights were obtained.

Key findings

- RM-GGBS based geopolymers of mixes (M2, M3, M4 and M5) exhibited higher compressive strength under ambient curing than under carbonation curing, indicating that strength development in systems containing RM is negatively impacted by carbonation. The strength increased as the GGBS content increased, despite the presence of small surface cracks and voids. Furthermore, under both curing regimes, the GGBS-based geopolymer mix (M6) demonstrated greater compressive strength than all other mixes; however, its strength varied with the molarity and curing conditions.
- In RM-containing mixes (M2, M3, M4 and M5), carbonated specimens showed lower compressive strength (8.15 - 14.8 MPa) than ambient cured samples (8.49 - 25.46 MPa), primarily due to preferential calcite formation, which hinders C-A-S-H gel development. However, GGBS-based systems showed better strength (43.22 MPa - 55.81 MPa) under carbonation curing, especially at higher molarities, owing to elevated calcium availability. Whereas ambient cured GGBS-based samples exhibited lower compressive strength than carbonation curing between 27.96 - 52.48 MPa. The existence of calcite and thermonatrite phases was verified by SEM and XRD, indicating significant carbonation.
- In general, ambient cured samples displayed a compact gel matrix with limited unreacted material as proven by the SEM micrographs and broad amorphous halo in the XRD spectra. This clearly indicates the absence of calcite formation accompanied by gel formation. Similar-way, carbonated cured GGBS-based geopolymer samples exhibited superior performance.
- Overall, the GGBS-based geopolymer specimens demonstrated superior mechanical strength due to high calcium content, which favours the development of strength and micro structural stability under carbonation curing.
- The production of C-A-S-H, N-A-S-H, and hybrid C-(N)-A-S-H gels in RM-GGBS systems is confirmed by EDS analysis. Higher Ca/Si and Si/Al ratios in GGBS-based system led to a denser and stronger matrix, whereas higher Na/Si ratios in RM-rich mixes indicate increased alkalinity and reactivity. Due to decalcification, carbonation curing lowers the Ca/Si ratio, which causes microstructural alterations such as microcracking and impairs overall performance.

- Thermogravimetric analysis (TGA) provided quantitative evidence of CO_2 sequestration through mass loss associated with carbonate decomposition in the temperature range of 550 - 850 ºC.
- RM-containing mixes showed a greater sequestration capability than GGBS-rich systems, according to the computed CO_2 uptake from TGA results, highlighting the important impact of alkalinity and pore structure in enhancing carbonation.
- The reduction in CO_2 uptake was observed in higher molarity of GGBS-based samples, likely due to the densification of matrix, which limits CO_2 diffusion, whereas RM-containing mixes maintained relatively higher CO_2 uptake.
- GGBS-rich systems show better CO_2 uptake only at low molarity under ambient curing, whereas RM-containing mixes demonstrate more consistent CO_2 uptake across different molarity levels
- CO_2 sequestration is governed by both curing conditions and mix composition, where RM-containing mixes exhibit consistently higher sequestration under both ambient and carbonation curing, whereas GGBS-based systems show effective carbonation primarily at lower molarity. Under carbonation curing, CO_2 uptake is further enhanced, particularly in RM-containing mixes, whereas higher molarity may reduce uptake due to matrix densification limiting CO_2 diffusion.

Final insight

- Carbonation curing effect depends on composition of the binder mix. It lowers strength in RM containing systems (M2, M3, M4 and M5) by hindering gel formation, but enhances strength in GGBS-based geopolymer systems, from calcite and C-A-S-H gel formation.
- TGA shows GGBS-rich mixes have medium CO_2 uptake with better densification and strength, whereas RM mixes have higher CO_2 uptake from more reactivity due to alkaline nature but exhibits lower strength.

Limitations

Despite the valuable insights obtained, this study has certain limitations.

- Thermogravimetric analysis was primarily used to determine the CO_2 sequestration, which may influence the accuracy of uptake calculation.
- These experiments might not provide a good reflection of long-term field performance and durability due to their being in a controlled laboratory environment and having a shorter curing time.
- SEM observations and ImageJ-based analysis were the primary methods used for microstructural characterization, which produced localized data without thorough pore structure quantification.

6. Future Scope

- Further studies are needed to determine the carbonations behaviour of RM-GGBS based systems for long-term, this is why the future research should focus on studying the long-term durability of the systems in different environmental conditions.
- Future research may explore methods to improve red mud activations in these RM-GGBS geopolymer systems to achieve better carbonation and mechanical properties.
- To make it practical and applicable, further studies are needed to perfect the parameters of carbonation curing and test it in the field in realistic conditions.
- It will need further studies to evaluate the stability and resistance of geopolymer systems based on carbonation cured GGBS to long-term exposure and environmental conditions.
- Also, the combination of GGBS-based binders and industrial CO2 capture systems should be explored to enhance sustainable use of carbon.
- Finally, a thorough life cycle assessment (LCA) and cost analysis would be needed to measure the environmental gain and determine the feasibility of a large-scale use as sustainable construction materials.

Declaration of Competing Interest

The authors declare that they have no known competing financial interests or personal relationships that could have appeared to influence the work reported in this paper.

CRediT authorship contribution statement

R Rani: Writing – original draft, Visualization, Validation, Methodology, Investigation, Conceptualization. M. Shanmugasundaram: Writing – review & editing, Supervision, Methodology, Conceptualization.

Acknowledgment

The authors express their gratitude to the Vellore Institute of Technology, Chennai, for the necessary support in implementing this work.

Data availability

Data will be made available on request.

References

A., T. & O.M., S. (2024) Investigation on the properties of sustainable alkali-activated GGBS mortar with nano silica and dredged marine sand: Mechanical, microstructural and durability aspects. *Case Studies in Construction Materials*. 20. doi:10.1016/j.cscm.2024.e03148.

Ahmad, J., Kontoleon, K.J., Majdi, A., Naqash, M.T., Deifalla, A.F., Ben Kahla, N., Isleem, H.F. & Qaidi, S.M.A. (2022) A Comprehensive Review on the Ground Granulated Blast Furnace Slag (GGBS) in Concrete Production. *Sustainability (Switzerland)*. 14 (14). doi:10.3390/su14148783.

Ahmed, O., Ahmad, S. & Adekunle, S.K. (2024) Carbon dioxide sequestration in cementitious materials: A review of techniques, material performance, and environmental impact. *Journal of CO2 Utilization*. 83. doi:10.1016/j.jcou.2024.102812.

Ai, T., Zhong, D., Zhang, Y., Zong, J., Yan, X. & Niu, Y. (2021) The effect of red mud content on the compressive strength of geopolymers under different curing systems. *Buildings*. 11 (7). doi:10.3390/buildings11070298.

Akhlaq, H., Peng, T., Ajmal, M.M., Khan, M.S. & Riaz, M. (2025) Impact of GGBS on the rheology and mechanical behavior of pumpable concrete. *Frontiers in Materials*. 12. doi:10.3389/fmats.2025.1614951.

Al-Bakri, A.Y., Ahmed, H.M. & Hefni, M.A. (2022) Cement Kiln Dust (CKD): Potential Beneficial Applications and Eco-Sustainable Solutions. *Sustainability (Switzerland)*.14 (12). doi:10.3390/su14127022.

Albayrak, E. & Özen, S. (2025) Enhancing geopolymer synthesis through calcination: Increasing the potential of natural material utilization. *Open Ceramics*. 22. doi:10.1016/j.oceram.2025.100796.

Amar, M., Ladduri, B., Alloul, A., Benzerzour, M. & Abriak, N.E. (2024) Geopolymer synthesis and performance paving the way for greener building material: A comprehensive study. *Case Studies in Construction Materials*. 20. doi:10.1016/j.cscm.2024.e03280.

Amari, S., Darestani, M., Millar, G.J., Samali, B. & Strounina, E. (2024) Engineering and Life Cycle Assessment (LCA) of Sustainable Zeolite-Based Geopolymer Incorporating Blast Furnace Slag. *Sustainability (Switzerland)*. 16 (1). doi:10.3390/su16010440.

An, Q., Pan, H., Zhao, Q. & Wang, D. (2022) Strength development and microstructure of sustainable geopolymers made from alkali-activated ground granulated blast-furnace slag, calcium carbide residue, and red mud. *Construction and Building Materials*. 356. doi:10.1016/j.conbuildmat.2022.129279.

Anon (2025) The Synergy of Low-NaOH Activation and Carbon Sequestration in Sustainable Red Mud Based Geopolymer. doi:10.30955/gnj.07964.

Azar, P., Patapy, C., Samson, G., Cussigh, F., Frouin, L. & Cyr, M. (2024) Effect of natural and accelerated carbonation on microstructure and pH of sodium carbonate alkali-activated slag. *Cement and Concrete Research*. 181. doi:10.1016/j.cemconres.2024.107525.

Bai, F., Bai, B., Chen, J., Nie, Q. & Liu, J. (2024) Development of an ambient cured high-strength red mud-based geopolymer through calcination activation. *Sustainable Chemistry and Pharmacy*. 42. doi:10.1016/j.scp.2024.101866.

Beltrame, N.A.M., Dias, R.L., Witzke, F.B. & Medeiros-Junior, R.A. (2023) Effect of carbonation curing on the physical, mechanical, and microstructural properties of metakaolin-based geopolymer concrete. *Construction and Building Materials*. 406. doi:10.1016/j.conbuildmat.2023.133403.

Bernal, S.A. (2016) Microstructural changes induced by CO2 exposure in alkali-activated slag/metakaolin pastes. *Frontiers in Materials*. 3. doi:10.3389/fmats.2016.00043.

Bernal, S.A., Provis, J.L., Rose, V. & Mejía De Gutierrez, R. (2011) Evolution of binder structure in sodium silicate-activated slag-metakaolin blends. *Cement and Concrete Composites*. 33 (1), 46–54. doi:10.1016/j.cemconcomp.2010.09.004.

Cao, R., Zhao, H., Liu, P., Xu, L., Jia, Z. & Zhang, S. (2026) Carbonation behavior of GGBS with different reactivity and its regulatory effects on early hydration performance in alkali-activated system. *Construction and Building Materials*. 512. doi:10.1016/j.conbuildmat.2026.145393.

Chandralega, V. & Shanmugasundaram, M. (2026) Influence of oxalic acid and seawater in iron-based binders: Correlating porosity with compressive strength through image processing. *Advances in Science and Technology Research Journal*. 20 (3), 129–147. doi:10.12913/22998624/213903.

Chandralega, V., Shanmugasundaram, M. & Stone, D. (2025) Enhancing the performance of iron-based binders with seawater and CO2 sequestration. *Case Studies in Construction Materials*. 22. doi:10.1016/j.cscm.2025.e04367.

Das, S., Saha, P., Prajna Jena, S. & Panda, P. (2022) Geopolymer concrete: Sustainable green concrete for reduced greenhouse gas emission – A review. *Materials Today: Proceedings*. 60, 62–71. doi:10.1016/j.matpr.2021.11.588.

Davidovits, J. (1988) *Geopolymers of the first generation: siliface-process, geopolymer*. https://www.researchgate.net/publication/304822628.

Davidovits, J. (1994) *Properties of Geopolymer Cements*. https://www.researchgate.net/publication/284651826.

Ding, C., Dong, W., Zhang, A., Wang, Z., Zhao, N., Chen, R. & Fu, H. (2021) Life cycle water footprint assessment of concrete production in Northwest China. *Water Policy*. 23 (5), 1211–1229. doi:10.2166/wp.2021.009.

Ettahiri, Y., Bouargane, B., Fritah, K., Akhsassi, B., Pérez-Villarejo, L., Aziz, A., Bouna, L., Benlhachemi, A. & Novais, R.M. (2023) A state-of-the-art review of recent advances in porous

geopolymer: Applications in adsorption of inorganic and organic contaminants in water. *Construction and Building Materials*.395. doi:10.1016/j.conbuildmat.2023.132269.

Fahim Huseien, G., Mirza, J., Ismail, M., Ghoshal, S.K. & Abdulameer Hussein, A. (2017) Geopolymer mortars as sustainable repair material: A comprehensive review. *Renewable and Sustainable Energy Reviews*.80 pp.54–74. doi:10.1016/j.rser.2017.05.076.

Firdous, R., Hirsch, T., Klimm, D., Lothenbach, B. & Stephan, D. (2021) Reaction of calcium carbonate minerals in sodium silicate solution and its role in alkali-activated systems. *Minerals Engineering*. 165. doi:10.1016/j.mineng.2021.106849.

Ganesan, Y. & Ravichandran, P.T. (2026) Development and performance of ambient cured geopolymer concrete with low alkali activation for sustainable construction. *Case Studies in Construction Materials*. 24, e06001. doi:10.1016/j.cscm.2026.e06001.

Gao, Y., Xu, W., Li, Y. & Liu, J. (2025) Early hydration and rheological behavior of carbide slag-activated red mud/GGBS Full waste grouting material. *Journal of Building Engineering*. 111. doi:10.1016/j.jobe.2025.113324.

Guo, S., Wang, H., Duan, Z., Zhang, H., Qian, H. & Ye, H. (2026) Effect of different reactive activators on the setting time and compressive strength of geopolymer in high-temperature environment. *Construction and Building Materials*. 518. doi:10.1016/j.conbuildmat.2026.145750.

H M, A.K. & M S, S. (2025) Durability and microstructure of fiber-reinforced geopolymer concrete with FA and GGBS. *Structures*. 71. doi:10.1016/j.istruc.2024.108096.

Hao, H., Liu, X., Dong, X., Li, J., Li, J., Xu, X. & Chang, S. (2025) Study on the optimal ratios and strength formation mechanism of mechanical activation red mud based geopolymer. *Journal of Building Engineering*. 104. doi:10.1016/j.jobe.2025.112401.

Harirchi, P. & Yang, M. (2022) Exploration of Carbon Dioxide Curing of Low Reactive Alkali-Activated Fly Ash. *Materials*. 15 (9). doi:10.3390/ma15093357.

H.M., T. & Unnikrishnan, S. (2023) Mechanical Strength and Microstructure of GGBS-SCBA based Geopolymer Concrete. *Journal of Materials Research and Technology*. 24, 7816–7831. doi:10.1016/j.jmrt.2023.05.051.

Hongwei, Y., Majdi, A., Ali, H.E. & Escorcia-Gutierrez, J. (2025) Green concrete alternatives: Utilizing industrial byproducts in geopolymer systems. *Case Studies in Construction Materials*. 23. doi:10.1016/j.cscm.2025.e05253.

Ilahi, K., Debbarma, S., Mathew, G. & Inyang, H.I. (2024) Carbon capture and mineralisation using red mud: A systematic review of its principles and applications. *Journal of Cleaner Production*.473. doi:10.1016/j.jclepro.2024.143458.

J, B.S. & P R, K.R. (2024) Effects of multiple precursors on strength, durability, and microstructural properties of ambiently cured geopolymer concrete. *Construction and Building Materials*. 442. doi:10.1016/j.conbuildmat.2024.137538.

Jin, W., Chen, Y., Lv, Y., Jiang, L., Bai, W., Zhang, K., Song, C. & Zhang, X. (2024) Mechanical Properties and Mechanism of Geopolymer Cementitious Materials Synergistically Prepared Using Red Mud and Yellow River Sand. *Materials*. 17 (15). doi:10.3390/ma17153810.

John, E., Chalapuram, K.M., Shebin, P., Mohan, H.K. & Frazana, Z. (2016) Geopolymer Concrete Using Red Mud and GGBS. *International Research Journal of Engineering and Technology*. www.irjet.net.

Jun, Y., Han, S.H. & Kim, J.H. (2024) Performance of CO2-cured alkali-activated blast-furnace slag incorporating magnesium oxide. *Construction and Building Materials*. 429. doi:10.1016/j.conbuildmat.2024.136462.

Jun, Y., Han, S.H. & Kim, J.H. (2023) Performance of CO2-Cured Alkali-Activated Slag Pastes During Curing and Exposure. *International Journal of Concrete Structures and Materials*. 17 (1). doi:10.1186/s40069-022-00563-3.

Kahyarian, A., Brown, B. & Nesic, S. (n.d.) *Mechanism of CO2 Corrosion of Mild Steel: a New Narrative*.

Kanyal, K.S., Agrawal, Y. & Gupta, T. (2021) Properties of Sustainable Concrete Containing Red Mud: A Review. *Journal of Scientific Research and Reports*. 15–26. doi:10.9734/jsrr/2021/v27i330366.

Konduru, H., Karthiyaini, S. & Shanmugasundaram, M. (2025) Comparative study of silica fume and sodium silicate as replacement of active reactive silica in bauxite residue based geopolymer mortar. *Case Studies in Construction Materials*. 22. doi:10.1016/j.cscm.2025.e04302.

Kopitha, K., Rajeev, P., Sanjayan, J. & Elakneswaran, Y. (2025) CO2 sequestration and low carbon strategies in 3D printed concrete. *Journal of Building Engineering*.99. doi:10.1016/j.jobe.2024.111653.

Koshy, N., Dondrob, K., Hu, L., Wen, Q. & Meegoda, J.N. (2019) Mechanical properties of geopolymers synthesized from fly ash and red mud under ambient conditions. *Crystals*. 9 (11). doi:10.3390/cryst9110572.

Kuandykova, A., Taimasov, B., Potapova, E., Sarsenbaev, B., Kolesnikov, A., Begentayev, M., Kuldeyev, E., Dauletiyarov, M., Zhanikulov, N., Amiraliyev, B. & Abdullin, A. (2024) Production of Composite Cement Clinker Based on Industrial Waste. *Journal of Composites Science*. 8 (7). doi:10.3390/jcs8070257.

Kumar, M., Kumar, A., Solanki, D. & Mungule, M. (2023a) Low molarity geopolymer concrete: Effects on compressive strength, elastic modulus, sorptivity and chloride migration. *Construction and Building Materials*. 409. doi:10.1016/j.conbuildmat.2023.134065.

Kumar, M., Kumar, A., Solanki, D. & Mungule, M. (2023b) Low molarity geopolymer concrete: Effects on compressive strength, elastic modulus, sorptivity and chloride migration. *Construction and Building Materials*. 409. doi:10.1016/j.conbuildmat.2023.134065.

Kumar Poloju, K. & Srinivasu, K. (2022) Influence of GGBS and concentration of sodium hydroxide on strength behavior of geopolymer mortar. In: *Materials Today: Proceedings*. 1 January 2022 Elsevier Ltd. pp. 702–706. doi:10.1016/j.matpr.2022.03.276.

Kurusta, T., Mucsi, G., Kumar, S. & Kristály, F. (2023) Carbon-dioxide sequestration by mechanical activation of Linz-Donawitz steel slag; the effect of water on CO2 capture. *Fuel*. 352. doi:10.1016/j.fuel.2023.128951.

Lamaa, G., Duarte, A.P.C., Silva, R.V. & de Brito, J. (2023) Carbonation of Alkali-Activated Materials: A Review. *Materials*.16 (8). doi:10.3390/ma16083086.

Lang, Y.-J., Yin, G.-J., Wen, X.-D., Miao, L., Gao, X.-J. & Cheng, S.-S. (2025) Research progress, hotspot evolution, and future trends of geopolymer concrete: A bibliometric review in the period 2000–2024. *Case Studies in Construction Materials*. 23, e05383. doi:10.1016/j.cscm.2025.e05383.

Li, B., Hu, J., Chen, L., Zhang, J. & Gu, J. (2025a) Strength and its microstructure evolution of GGBS-FA geopolymer mortar under seawater. *Case Studies in Construction Materials*. 22. doi:10.1016/j.cscm.2025.e04662.

Li, Y., Xu, W., Gao, Y. & Liu, J. (2025b) Development of full solid waste-based grouting materials using calcium carbide slag-activated red mud/GGBS. *Construction and Building Materials*. 483. doi:10.1016/j.conbuildmat.2025.141827.

Li, Z., Dong, H., Zhao, X., Wang, K. & Gao, X. (2025c) Utilisation of Bayer red mud for high-performance geopolymer: Competitive roles of different activators. *Case Studies in Construction Materials*. 23. doi:10.1016/j.cscm.2025.e05047.

Li, Z., Gao, M., Lei, Z., Tong, L., Sun, J., Wang, Y., Wang, X. & Jiang, X. (2023) Ternary cementless composite based on red mud, ultra-fine fly ash, and GGBS: Synergistic utilization and geopolymerization mechanism. *Case Studies in Construction Materials*. 19. doi:10.1016/j.cscm.2023.e02410.

Li, Z. & Ikeda, K. (2024) Compositions and Microstructures of Carbonated Geopolymers with Different Precursors. *Materials*. 17 (7). doi:10.3390/ma17071491.

Li, Z., You, H., Gao, Y., Wang, C. & Zhang, J. (2021) Effect of ultrafine red mud on the workability and microstructure of blast furnace slag-red mud based geopolymeric grouts. *Powder Technology*. 392, 610–618. doi:10.1016/J.POWTEC.2021.07.046.

Liang, X. & Ji, Y. (2021) Mechanical properties and permeability of red mud-blast furnace slag-based geopolymer concrete. *SN Applied Sciences*. 3 (1). doi:10.1007/s42452-020-03985-4.

Liu, H. & Li, Q. (2023) Preparation of artificial aggregates from concrete slurry waste and waste brick masonry powder: CO2 uptake and performance evaluation. *Construction and Building Materials*. 382. doi:10.1016/j.conbuildmat.2023.131356.

Liu, J., Ren, Y., Li, Z., Niu, R., Xie, G., Zhang, W. & Xing, F. (2024a) Efflorescence and mitigation of red mud–fly ash–phosphogypsum multicomponent geopolymer. *Construction and Building Materials*. 448. doi:10.1016/j.conbuildmat.2024.137869.

Liu, P., Zhong, J., Zhang, M., Mo, L. & Deng, M. (2021) Effect of CO2 treatment on the microstructure and properties of steel slag supplementary cementitous materials. *Construction and Building Materials*. 309. doi:10.1016/j.conbuildmat.2021.125171.

Liu, R., Li, X., Zhang, Z. & Zhang, X. (2024b) Effect of ground granulated blast-furnace slag (GGBS) and sulphoaluminate cement (SAC) on the strength and microstructure of ordinary Portland cement paste at elevated temperatures. *Powder Technology*. 448. doi:10.1016/j.powtec.2024.120226.

Liu, S., Shen, Y., Wang, Y., Shen, P., Xuan, D., Guan, X. & Shi, C. (2022) Upcycling sintering red mud waste for novel superfine composite mineral admixture and CO2 sequestration. *Cement and Concrete Composites*. 129. doi:10.1016/j.cemconcomp.2022.104497.

Luo, Y. & He, D. (2021) Research status and future challenge for CO2 sequestration by mineral carbonation strategy using iron and steel slag. *Environmental Science and Pollution Research*.28 (36) pp.49383–49409. doi:10.1007/s11356-021-15254-x.

Lyu, J., Zhao, S., Xing, C., Wang, C., Chu, G., Xi, X., Zhou, C., Song, L., Ma, K. & Yue, H. (2024) The production of artificial aggregates with flue gas desulfurization ash: Development of a novel carbonation route. *Journal of Cleaner Production*. 444. doi:10.1016/j.jclepro.2024.141068.

Mariyappan, V. & Somasundaram, K. (2025) The Synergy of Low-NaOH Activation and Carbon Sequestration in Sustainable Red Mud Based Geopolymer. *Global Nest Journal*. 27 (9). doi:10.30955/gnj.07964.

Meshram, R.B., Mohapatra, A., Malakar, S., Gupta, P.K., Sahoo, D.P., Nath, S.K., Alex, T.C. & Kumar, S. (2024) Environmental impact analysis of geopolymer based red mud paving blocks. *Discover Applied Sciences*. 6 (10). doi:10.1007/s42452-024-06253-x.

Mishra, J., Nanda, B., Patro, S.K. & Krishna, R.S. (2024a) A comprehensive review on compressive strength and microstructure properties of GGBS-based geopolymer binder systems. *Construction and Building Materials*.417. doi:10.1016/j.conbuildmat.2024.135242.

Mishra, J., Nanda, B., Patro, S.K. & Krishna, R.S. (2024b) A comprehensive review on compressive strength and microstructure properties of GGBS-based geopolymer binder systems. *Construction and Building Materials*.417. doi:10.1016/j.conbuildmat.2024.135242.

Mohamed, A.M., Tayeh, B.A., Majeed, S.S., Aisheh, Y.I.A. & Salih, M.N.A. (2024) Fresh, hardened, durability and microstructure properties of seawater concrete: A systematic review. *Journal of CO2 Utilization*. 83. doi:10.1016/j.jcou.2024.102815.

Mohammed, T.O., Singh, D. & Fanijo, E.O. (2025) Calcium Carbide Residue as a Supplementary Precursor is Geopolymer Binders. *Frontiers in Materials*. 12. doi:10.3389/fmats.2025.1718575.

Moro, D., Fabbri, R., Romano, J., Ulian, G., Calafato, A., Solouki, A., Sangiorgi, C. & Valdrè, G. (2021) Thermal, X-ray diffraction and oedometric analyses of silt-waste/NaOH-activated metakaolin geopolymer composite. *Journal of Composites Science*. 5 (10). doi:10.3390/jcs5100269.

Mudgal, M., Singh, A., Chouhan, R.K., Acharya, A. & Srivastava, A.K. (2021a) Fly ash red mud geopolymer with improved mechanical strength. *Cleaner Engineering and Technology*. 4. doi:10.1016/j.clet.2021.100215.

Mudgal, M., Singh, A., Chouhan, R.K., Acharya, A. & Srivastava, A.K. (2021b) Fly ash red mud geopolymer with improved mechanical strength. *Cleaner Engineering and Technology*. 4. doi:10.1016/j.clet.2021.100215.

Munir, Q., Abdulkareem, M., Horttanainen, M. & Kärki, T. (2023) A comparative cradle-to-gate life cycle assessment of geopolymer concrete produced from industrial side streams in comparison with traditional concrete. *Science of the Total Environment*. 865. doi:10.1016/j.scitotenv.2022.161230.

Nguyen, T.T., Goodier, C.I. & Austin, S.A. (2020) Factors affecting the slump and strength development of geopolymer concrete. *Construction and Building Materials*. 261. doi:10.1016/j.conbuildmat.2020.119945.

Nicula, L.M., Manea, D.L., Simedru, D., Cadar, O., Dragomir, M.L., Ardelean, I. & Corbu, O. (2023) Potential Role of GGBS and ACBFS Blast Furnace Slag at 90 Days for Application in Rigid Concrete Pavements. *Materials*. 16 (17). doi:10.3390/ma16175902.

Nie, Q., Hu, W., Ai, T., Huang, B., Shu, X. & He, Q. (2016) Strength properties of geopolymers derived from original and desulfurized red mud cured at ambient temperature. *Construction and Building Materials*. 125, 905–911. doi:10.1016/j.conbuildmat.2016.08.144.

Osio-Norgaard, J., Gevaudan, J.P. & Srubar, W. V. (2018) A review of chloride transport in alkali-activated cement paste, mortar, and concrete. *Construction and Building Materials*.186 pp.191–206. doi:10.1016/j.conbuildmat.2018.07.119.

Ozcelikci, E., Kul, A., Gunal, M.F., Ozel, B.F., Yildirim, G., Ashour, A. & Sahmaran, M. (2023) A comprehensive study on the compressive strength, durability-related parameters and microstructure of geopolymer mortars based on mixed construction and demolition waste. *Journal of Cleaner Production*. 396. doi:10.1016/j.jclepro.2023.136522.

Pan, S.Y., Chiang, A., Chang, E.E., Lin, Y.P., Kim, H. & Chiang, P.C. (2015) An innovative approach to integrated carbon mineralization and waste utilization: A review. *Aerosol and Air Quality Research*.15 (3) pp.1072–1091. doi:10.4209/aaqr.2014.10.0240.

Peng, G.F., Wang, X.F., Ding, H. & Jia, Y.J. (2025) Effect of calcined red mud on the mechanical properties and microstructure of ultra-high performance concrete. *Construction and Building Materials*. 484. doi:10.1016/j.conbuildmat.2025.141891.

Polettini, A., Pomi, R. & Stramazzo, A. (2016) Carbon sequestration through accelerated carbonation of BOF slag: Influence of particle size characteristics. *Chemical Engineering Journal*. 298, 26–35. doi:10.1016/j.cej.2016.04.015.

Qingke, N., Haiqing, Z., Haipeng, Y., Xiangxin, J. & Rihua, Z. (2024) Development and field test of Red mud-Fly Ash Geopolymer pile (RFP). *Cleaner Waste Systems*. 9. doi:10.1016/j.clwas.2024.100184.

Ram Kumar, B.A.V. & Ramakrishna, G. (2023) Performance evaluation of red mud as a construction material – A review. *Materials Today: Proceedings*. doi:10.1016/j.matpr.2023.04.043.

Raza, A., Selmi, A., Elhadi, K.M., Ghazouani, N. & Chen, W. (2024) Strength analysis and microstructural characterization of calcined red mud based-geopolymer concrete modified with slag and phosphogypsum. *Journal of Materials Research and Technology*. 33, 6168–6181. doi:10.1016/j.jmrt.2024.10.248.

Saranya, V., Karthiyaini, S. & Stone, D. (2025) Enhancement of strength and microstructural characterization in red mud-iron carbonate binders: Effects of CO2 sequestration and oxalic acid concentration. *Results in Engineering*. 25. doi:10.1016/j.rineng.2025.104539.

Sasui, S., Kim, G., van Riessen, A., Lim, C., Eu, H., Park, J. & Nam, J. (2024) Effects of Na2SiO3/NaOH ratio in alkali activator on the microstructure, strength and chloride ingress in fly ash and GGBS based alkali activated concrete. *Journal of Building Engineering*. 98. doi:10.1016/j.jobe.2024.111255.

Shamsah, M., Kalfat, R. & Subramaniam, K.V.L. (2025) Impact of low NaOH molarities on mechanical and durability properties of ambient and oven-cured fly ash geopolymer concrete. *Journal of Building Engineering*. 105. doi:10.1016/j.jobe.2025.112491.

Simha, B., Yeddula, R. & Somasundaram, K. (2020) Effect of red mud proportion on the strength and microstructure of ferrosialate based geopolymer mortar. *Indian Journal of Engineering & Materials Sciences*.27.

Standard, I. (2021) *Hardened Concrete-Methods of Test Part 1 Testing of Strength of Hardened Concrete Section 1 Compressive, Flexural and Split Tensile Strength (First Revision)*. www.standardsbis.in.

Sun, D.M., M, B. & Saji, J. (2026) Sustainable synergies: Performance evaluation of cement mortar with red mud and industrial by- products. *Next Materials*. 10. doi:10.1016/j.nxmate.2025.101479.

Sun, T., Peng, R., Alrefaei, Y., Xian, X. & Wang, Y. (2025) Influence of carbonation initiation timing on CO2 uptake and mechanical performance of geopolymer made from ternary solid wastes. *Construction and Building Materials*. 498. doi:10.1016/j.conbuildmat.2025.144033.

Thonemann, N., Zacharopoulos, L., Fromme, F. & Nühlen, J. (2022) Environmental impacts of carbon capture and utilization by mineral carbonation: A systematic literature review and meta life cycle assessment. *Journal of Cleaner Production*.332. doi:10.1016/j.jclepro.2021.130067.

Tran, N.P., Sani, M.A., Nguyen, T.N. & Ngo, T.D. (2024) Microstructure and pore structure of one-part geopolymer incorporating electrolytic copper powder and graphene oxide. *Construction and Building Materials*. 456. doi:10.1016/j.conbuildmat.2024.139331.

Tripathy, A. & Acharya, P.K. (2023) Effect of normal, blended and geopolymer concrete on ecosystem. *Materials Today: Proceedings*. doi:10.1016/j.matpr.2023.05.079.

Uysal, M., Dilbas, H., Çoşgun, T. & Bendjilali, F. (2024) Red-mud additive geopolymer composites with eco-friendly aggregates. *Construction and Building Materials*. 425. doi:10.1016/j.conbuildmat.2024.135915.

Vashistha, P., Oinam, Y. & Pyo, S. (2023) Valorization of waste concrete powder (WCP) through silica fume incorporation to enhance the reactivity and hydration characteristics. *Developments in the Built Environment*. 16. doi:10.1016/j.dibe.2023.100272.

Venkatachalam, S. & Somasundaram, K. (2026) Adverse effect on the strength and microstructural characteristics of iron-based binders under the influence of initial atmospheric exposure before CO2 curing. *Advances in Science and Technology Research Journal*. 20 (1), 222–235. doi:10.12913/22998624/211126.

Venkatesh, V. & Shanmugasundaram, M. (2024) Enhancement of mechanical and microstructural characteristics of magnesium oxychloride cement with metasteatite. *Case Studies in Construction Materials*. 21. doi:10.1016/j.cscm.2024.e03683.

Vignesh, J., Ramesh, B. & Xavier, J.R. (2025) A comprehensive review of materials, processing, and performance of nano-doped engineered geopolymer composites for construction applications. *Case Studies in Construction Materials*. 23. doi:10.1016/j.cscm.2025.e05625.

Vogrin, J., Santini, T., Peng, H. & Vaughan, J. (2020) Influence of chloride on sodium aluminosilicate solubility in Bayer liquor. *Microporous and Mesoporous Materials*. 299. doi:10.1016/j.micromeso.2020.110086.

Wang, L. & Fan, Y. (2025) Carbon sequestration technology in concrete: A review of mechanism, application and optimization strategy. *Journal of Building Engineering*.102. doi:10.1016/j.jobe.2025.111862.

Wang, S., Kim, J. & Qin, T. (2024) Mineral carbonation of iron and steel by-products: State-of-the-art techniques and economic, environmental, and health implications. *Journal of CO2 Utilization*.81. doi:10.1016/j.jcou.2024.102707.

Wang, Z. & Ma, S. (2024) 06227 Copyright© 2024 Global NEST Printed in Greece. All rights reserved Zhiqiang Wang and Shenglin Ma (2024), Research on. *Global NEST Journal*. 26 (7), 6227. doi:10.30955/gnj.006227.

Wang, Z., Wu, Q. & Ma, S. (2024) carbon emission peaks in large energy production region in China-Based on the open stirpat model Research on carbon emission peaks in large energy production region in China-Based on the open stirpat model. *Global NEST Journal*. 26 (5), 6121. doi:10.30955/gnj.006121.

Werling, N., Dehn, F., Krause, F., Steudel, A., Schuhmann, R. & Emmerich, K. (2020) SOLUBILITY OF PRECURSORS AND CARBONATION OF WATERGLASS-FREE GEOPOLYMERS. *Clays and Clay Minerals*. 68 (5), 524–531. doi:10.1007/s42860-020-00096-4.

Winnefeld, F., Leemann, A., German, A. & Lothenbach, B. (2022) CO2 storage in cement and concrete by mineral carbonation. *Current Opinion in Green and Sustainable Chemistry*.38. doi:10.1016/j.cogsc.2022.100672.

Wu, P., Wei, C., Liu, X., Zhang, Z., Xue, Y. & Liu, X. (2025) Impact of hematite in red mud on hydration characteristics and environmental performance of cementitious materials. *Cement and Concrete Composites*. 160. doi:10.1016/j.cemconcomp.2025.106035.

Wu, X., Zhou, X., Guo, C., Kang, D., Zhang, W., Lan, J. & Fang, Z. (2024) Behavior of hematite, magnetite, and reduced iron powder in geopolymers: Effects of mechanical properties and reaction mechanism. *Journal of Cleaner Production*. 444. doi:10.1016/j.jclepro.2024.141178.

Xia, W., Ruan, Z., Ma, S., Zhao, J. & Yan, J. (2025) Can the digital economy enhance carbon emission efficiency? Evidence from 269 cities in China. *International Review of Economics and Finance*. 97. doi:10.1016/j.iref.2024.103815.

Yang, D., Wang, P., Chen, W., Liu, L., Huang, Y., Xiang, X., Wang, G. & Wu, J. (2025) Effects of red mud, desert sand, and ground granulated blast furnace slag on the mechanical properties and microstructure of fly ash-based geopolymer. *Construction and Building Materials*. 468. doi:10.1016/j.conbuildmat.2025.140471.

Yeddula, B.S.R. & Karthiyaini, S. (2020a) Experimental investigations and GEP modelling of compressive strength of ferrosialate based geopolymer mortars. *Construction and Building Materials*. 236. doi:10.1016/j.conbuildmat.2019.117602.

Yeddula, B.S.R. & Karthiyaini, S. (2020b) Experimental Investigations and Prediction of Thermal Behaviour of Ferrosialate-Based Geopolymer Mortars. *Arabian Journal for Science and Engineering*. 45 (5), 3937–3958. doi:10.1007/s13369-019-04314-7.

Yue, Z., Dhandapani, Y. & Bernal, S.A. (2025) Structural alterations in alkali-sulfate-activated slag cement pastes induced by natural and accelerated carbonation. *Cement and Concrete Research*. 187. doi:10.1016/j.cemconres.2024.107713.

Zakira, U., Zheng, K., Xie, N. & Birgisson, B. (2023) Development of high-strength geopolymers from red mud and blast furnace slag. *Journal of Cleaner Production*. 383. doi:10.1016/j.jclepro.2022.135439.

Zayed, A.M., Masoud, M.A., Rashad, A.M., El-Khayatt, A.M., Sakr, K., Kansouh, W.A. & Shahien, M.G. (2020) Influence of heavyweight aggregates on the physico-mechanical and radiation attenuation properties of serpentine-based concrete. *Construction and Building Materials*. 260. doi:10.1016/j.conbuildmat.2020.120473.

Zhang, D., Feng, B., Jaworska, B., Ellis, B.R., Fancy, S., Sick, V. & Li, V.C. (2025a) Pilot-scale validation of CO2 utilization for greener and tougher infrastructure through carbonation curing of bendable concrete. *Journal of Cleaner Production*. 491. doi:10.1016/j.jclepro.2025.144845.

Zhang, G., Ma, S., Zheng, M., Li, C., Chang, F. & Zhang, F. (2025b) Impact of digitization and artificial intelligence on carbon emissions considering variable interaction and heterogeneity: An interpretable deep learning modeling framework. *Sustainable Cities and Society*. 125. doi:10.1016/j.scs.2025.106333.

Zhang, T., Hu, K., Chen, Y., Lv, Y., Xue, X. & Qiao, P. (2025c) A wet carbonation enhancement approach to synergistic preparation of alkali-activated artificial aggregates from waste concrete powder and ground granulated blastfurnace slag. *Construction and Building Materials*. 486. doi:10.1016/j.conbuildmat.2025.142012.

Zhang, T., Hu, K., Chen, Y., Lv, Y., Xue, X. & Qiao, P. (2025d) A wet carbonation enhancement approach to synergistic preparation of alkali-activated artificial aggregates from waste concrete powder and ground granulated blastfurnace slag. *Construction and Building Materials*. 486. doi:10.1016/j.conbuildmat.2025.142012.

Zhang, W., Gao, R., Sha, X., Liu, G., Wang, X.Y., Lin, R.S. & Tong, Y. (2025e) Strength development and thermal stability analysis of carbonation-cured red mud-based cementitious materials. *Construction and Building Materials*. 470. doi:10.1016/j.conbuildmat.2025.140724.

Zhang, W., Gao, R., Sha, X., Liu, G., Wang, X.Y., Lin, R.S. & Tong, Y. (2025f) Strength development and thermal stability analysis of carbonation-cured red mud-based cementitious materials. *Construction and Building Materials*. 470. doi:10.1016/j.conbuildmat.2025.140724.

Zhang, X., Wang, X., Zhan, Q. & Song, C. (2024) Carbonation reaction properties and reaction mechanisms of red mud under different carbon dioxide pressures. *Journal of Environmental Chemical Engineering*. 12 (3). doi:10.1016/j.jece.2024.112910.

Zhao, Y., Lu, D., Fang, Z., Gao, Y., He, W., Han, Y., Jia, Q. & Zhang, B. (2025) Preparation of CO2 sequestration materials from semi-dry carbonized carbide slag and coal gasification slag: Study on carbon fixation performance of multistage carbonation. *Case Studies in Construction Materials*. 23. doi:10.1016/j.cscm.2025.e05255.

Zhou, W., Shi, X., Lu, X., Qi, C., Luan, B. & Liu, F. (2020) The mechanical and microstructural properties of refuse mudstone-GGBS-red mud based geopolymer composites made with sand. *Construction and Building Materials*. 253. doi:10.1016/j.conbuildmat.2020.119193.

Zhu, J., Yue, H., Ma, L., Li, Z. & Bai, R. (2023) The synergistic hydration mechanism and environmental safety of multiple solid wastes in red mud-based cementitious materials. *Environmental Science and Pollution Research*. 30 (32), 79241–79257. doi:10.1007/s11356-023-27800-w.